iScience

CellPress
OPEN ACCESS

Article

Thermodynamic Surface Analyses to Inform Biofilm Resistance

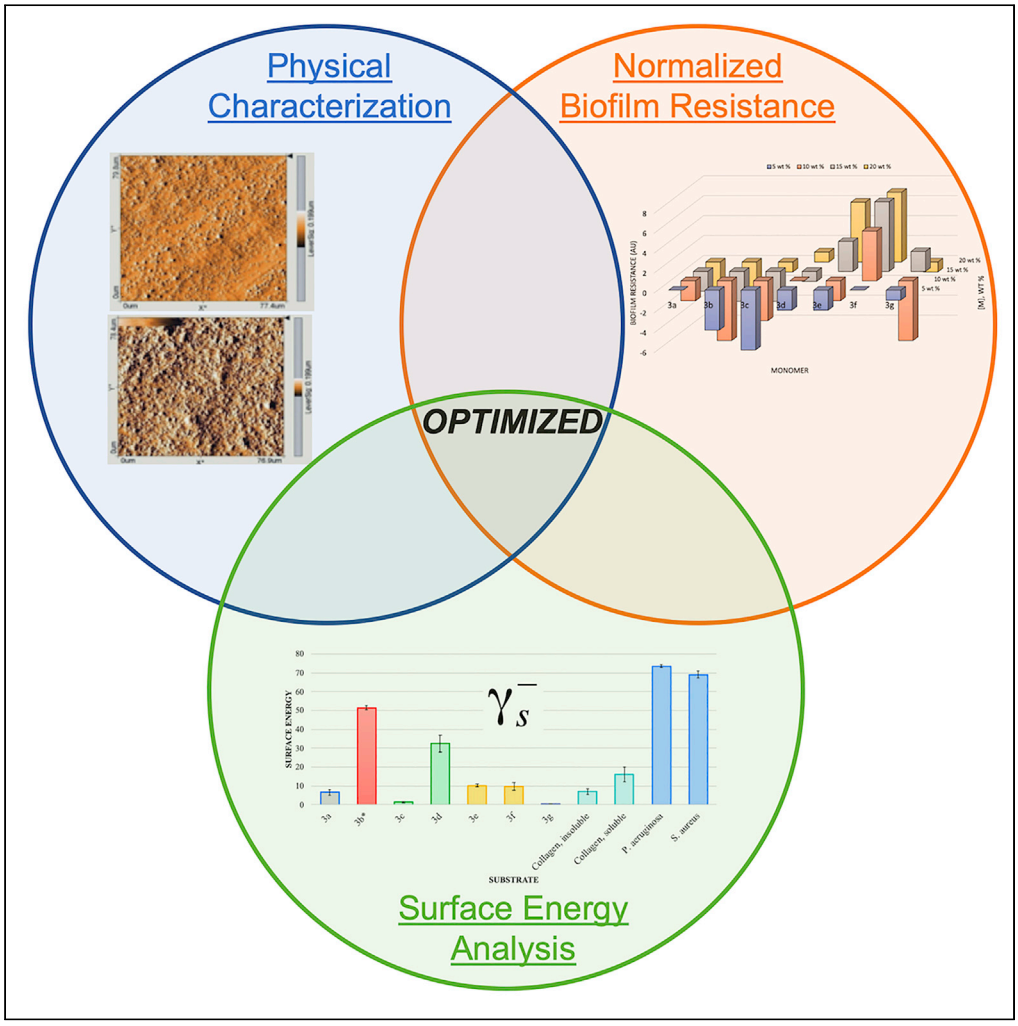

T. Brian Cavitt, Jasmine G. Carlisle, Alexandra R. Dodds, ..., Pooja R. Patel, Devin Smith, Wenting Wei

tbcavitt@lipscomb.edu

HIGHLIGHTS

Surface energy components affect bacterial adhesion to substrates

Bacterial adhesion is directly related to the substrate's polar component

Bacterial adhesion is inversely related to the substrate's base component

Polarizable substrates may allow bacterial association, and not adhesion

Cavitt et al., iScience *23*, 101702
November 20, 2020
https://doi.org/10.1016/j.isci.2020.101702

iScience

CellPress
OPEN ACCESS

Article

Thermodynamic Surface Analyses to Inform Biofilm Resistance

T. Brian Cavitt,[1,2,3,*] Jasmine G. Carlisle,[1] Alexandra R. Dodds,[2] Rebecca A. Faulkner,[2] Tyson C. Garfield,[2] Verena N. Ghebranious,[1] Phillip R. Hendley,[2] Emily B. Henry,[1] Charles J. Holt,[2] Jordan R. Lowe,[2] Jacob A. Lowry,[2] D. Spencer Oskin,[1] Pooja R. Patel,[1] Devin Smith,[2] and Wenting Wei[1]

SUMMARY

Biofilms are the habitat of 95% of bacteria successfully protecting bacteria from many antibiotics. However, inhibiting biofilm formation is difficult in that it is a complex system involving the physical and chemical interaction of both substrate and bacteria. Focusing on the substrate surface and potential interactions with bacteria, we examined both physical and chemical properties of substrates coated with a series of phenyl acrylate monomer derivatives. Atomic force microscopy (AFM) showed smooth surfaces often approximating surgical grade steel. Induced biofilm growth of five separate bacteria on copolymer samples comprising varying concentrations of phenyl acrylate monomer derivatives evidenced differing degrees of biofilm resistance via optical microscopy. Using goniometric surface analyses, the van Oss-Chaudhury-Good equation was solved linear algebraically to determine the surface energy profile of each polymerized phenyl acrylate monomer derivative, two bacteria, and collagen. Based on the microscopy and surface energy profiles, a thermodynamic explanation for biofilm resistance is posited.

INTRODUCTION

Biofilms allow the vast majority of microorganisms—infectious or otherwise—to persist in our world of antibiotics and antivirals. Biofilms are a complex, communicative aggregation of microorganisms in which 99% of all microorganisms persist (Flemming, 2002). Because of the ubiquitous nature of biofilms, their influence is similarly widespread—from biofouling of naval vessels, drinking and wastewater treatment facilities, medical implants and inserts to persistent pathogenic pathways in health care including nosocomial infections (Abbott et al., 2000; Cavitt and Faulkner, 2015, 2017; Cleaveland, 2005; Cooney and Tang, 1999; Flemming, 2002; Iwamoto and Matsutomo, 2018; Kenawy et al., 2007; Monroe, 2007; Montanaro et al., 2007; O'Flaherty et al., 2004; Vertes et al., 2012). Likewise, biofilms are non-trivial in remediation methods and often require multiple modalities to simply reduce and impede biofilm growth. With the inherent difficulty of biofilm remediation, research is moving toward inhibiting biofilm growth and/or formation.

Developing methods to inhibit biofilm growth and/or formation requires an intimate knowledge of the growth mechanism, which is parsed into five distinct categories: (1) primary colonization with reversible attachment, (2) aggregation and irreversible attachment, (3) growth and division, (4) maturation, and (5) dispersion (Monroe, 2007; Vertes et al., 2012). The most logical moment to disrupt biofilm formation is primary colonization in which microorganisms initially contact and reversibly adhere to a substrate's surface. Primary colonization is a multi-determinant system based on the thermodynamic (i.e., static) and kinetic (i.e., dynamic) nature of both microorganism and substrate.

One commonly investigated kinetic determinant involves the concentration dependence of biofilm inhibition. At a critical concentration (i.e., minimum inhibitory concentration [MIC]), biofilm growth is inhibited without introducing a cidal mechanism. The MIC likely addresses the kinetic effect based on the reversible attachment at primary colonization. At larger critical concentrations (i.e., minimum biocidal concentration [MBC]), a thermodynamic, cidal effect introduces disruptors to basic cellular function and, over time, shifts the microbial equilibrium away from homeostasis. Most commonly, biofilm inhibitory concentrations are in excess of the MBC with the thought that both kinetic and thermodynamic effects would be simultaneously

[1]Lipscomb University, Department of Chemistry and Biochemistry, One University Park Drive, Nashville, TN 37204, USA

[2]Abilene Christian University, Department of Chemistry and Biochemistry, ACU Box 28132, Abilene, TX 79699-8132, USA

[3]Lead Contact

*Correspondence: tbcavitt@lipscomb.edu

https://doi.org/10.1016/j.isci.2020.101702

addressed. As a motile species, *Pseudomonas aeruginosa* is likely most affected by the MIC-related kinetic effect, whereas the non-motile *Staphylococcus aureus* would be more affected by the MBC-related thermodynamic effect.

Introducing antimicrobial components to the substrate is a very common method to inhibit biofilm formation; however, such focuses on the previously described concentration determinant. Substrates are often functionalized with quaternary ammonium compounds (e.g., polymeric, polymer-grafted) in excess of MBC that penetrate the cell wall causing leakage and subsequent apoptosis (Kandiyote et al., 2019; Namivandi-Zangeneh et al., 2020; Valarikova et al., 2020). Upon apoptosis and in the absence of interfacial shear flow, the apoptotic fluids often remain associated with the substrate surface dynamically altering the nature of the substrate by concealing the quaternary ammonium under cellular debris. Furthermore, upon cell death, subsequent activation of lysosomes, and release of proteases, putrefaction of cellular proteins will produce free amines that neutralize protonated quaternary ammonium salts used in some of the aforementioned examples. The use of phenolic compounds to denature proteins necessary for cellular function are also common; unfortunately, like protonated quaternary ammonium compounds, the phenolic compounds are biocidal for a time until cellular debris and/or neutralization by free amines render them inert pending surface treatment (Li et al., 2020; Namivandi-Zangeneh et al., 2020). Other more robust compounds are also used to disrupt biofilm growth such as sugar alcohols to prevent dental caries and substituted (e.g., fluoro, chloro, nitro, cyano) aryl hydrazones (Kõljalg et al., 2020; Lu et al., 2020).

Using metals associated with the substrate to disrupt cellular function is also a common method of biofilm inhibition. Nanoparticles (e.g., silver) are of peculiar interest for thermodynamically mediated biofilm inhibition and have enhanced efficacy when employed with a secondary antimicrobial component (Moola et al., 2019; Namasivayam et al., 2019). However, nanoparticles often cannot endure rigorous surface treatments to recondition surfaces after eventual biofilm formation and/or fouling. Metal salts (e.g., Ce(IV)) have been shown to disrupt saccharide-dependent biofilm formation during the kinetically controlled reversible adhesion of primary colonization (Bhatt et al., 2020). However, metal salts often do not persist long term in aqueous environments thereby rendering them inactive.

Because of (1) significant genetic differentiation between microorganisms and (2) the colloidal nature of microorganisms, even adhesion is a complex process that is phenotypically heterogeneous and not a single determinant process (Vissers et al., 2019). For example, the surface protein SdrC of *S. aureus* has been shown to use Ca^{2+}-mediated chelation of the N2 domains as a primary contributor to biofilm formation; the use of a metal salt associated with the substrate may disrupt the aforementioned chelation illustrating how metal salts effectively inhibit biofilm formation (Pi et al., 2020). To further illustrate the diversity in the adhesion process, McLay et al. were able to genetically alter *Escherichia coli* to demonstrate that the amount of fimbriation contributes to adhesion of the bacterium (McLay et al., 2018). The concentration dependence of adhesion is probably a kinetic effect unique to each bacterium.

In a paper examining *P. aeruginosa* and its interfacial behavior, Deng et al. noted that most bacteria align parallel to the oil-water interface (Deng et al., 2020). The parallel alignment is likely thermodynamically driven, whereas non-parallel alignment is kinetically controlled. The kinetic (i.e., dynamic) component has been modeled using complex algorithms and applied theories to describe bacterial attachment (Conrad and Poling-Skutvik, 2018; McLay et al., 2018; Vissers et al., 2019).

In this paper, we primarily focus on the thermodynamic components that drive the interfacial interaction of substrates with microbes present in primary colonization. Our fundamental assumption throughout our biological experimentation is that biofilm growth cannot occur without primary colonization. Although we are not explicitly studying primary colonization, we are examining the results of microbial colonization that are possible only if primary colonization occurs via a significant substrate-bacteria interfacial interaction, an interaction that is limited in the latter stages of biofilm growth. Therefore, seven phenyl acrylate monomers, including six halogenated monomers, were synthesized and characterized. The substrate was coated with a formulation that included 5–20 weight percent of a phenyl acrylate derivative and subsequently polymerized. Using atomic force microscopy (AFM), the surface smoothness was determined for representative samples and compared with surgical grade steel. Induced single species biofilm growth and separate exposure to clarified sewage provided biological evidence of biofilm inhibition relative to each of the seven phenyl acrylate derivatives at varying concentrations. After solving the van Oss-Chaudhury-Good

Entry	$R^1/R^2/R^3$(2)	3	Yield (%)[a]
1	H/H/H(**2a**)	**3a**	59
2	H/Cl/H(**2b**)	**3b**	33
3	H/H/Cl(**2c**)	**3c**	36
4	Cl/H/Cl(**2d**)	**3d**	30.
5	H/H/Br(**2e**)	**3e**	21
6	Br/H/Br(**2f**)	**3f**	39
7	H/H/I(**2g**)	**3g**	<10

Table 1. Employing Different Phenols

Reaction conditions: **1** (55 mmol), **2** (50. mmol), Et_3N (55 mmol) in CH_2Cl_2 (40 mL) at room temperature and under dry nitrogen atmosphere for 24 h with spectroscopic and physical characterization provided in Data S1 and S2.

See also Figure S9.

[a]Yields refer to average isolated yields.

equation via a linear algebraic method for relevant samples, surface energy analyses and comparison of each polymerized phenyl acrylate derivative to collagen and two representative bacteria (e.g., *P. aeruginosa* and *S. aureus*) inform potential thermodynamic efficacy. Thereafter, a thermodynamic explanation for the observed behavior was posited based on the evidence gathered.

RESULTS AND DISCUSSION

Development of Potential Biofilm-Resistant Polymer Materials

Given evidence that covalently bound halogenated moieties have demonstrated efficacy for biofilm resistance, we designed a series of monomers based on phenyl acrylate (an internal control) that are likely biofilm-resistant candidates (Pickens, 2009). Table 1 details the reaction scheme and phenyl acrylate derivatives synthesized (see Transparent Methods). Impurities in acryloyl chloride (**1**), technical grade (70% purity), contributed in part to the low to moderate average isolated yields (Cavitt and Faulkner, 2015, 2017).

Monomers were shown to be stable upon exposure to broad spectrum UV radiation indicating that the aryl–halogen bonds persist upon irradiation thereto. Photo-differential scanning calorimetry (photo-DSC) was used to confirm that the aryl-halogen bond does not undergo homolytic cleavage to initiate polymerization at 10 weight percent of each monomer as compared with 1,6-hexanediol diacrylate. The aforementioned stability allowed for UV curing of the monomer to form both homo- and copolymeric coatings on several substrates (e.g., stainless steel, glass slides, and plastic slides) for subsequent analyses. The monomers were incorporated at 5, 10, 15, and 20 weight percent into a standard copolymer formulation. Each liquid coating was manually drawn down to a wet thickness of 100 μm and polymerized thereafter.

Samples of the cured 20% monomer formulation were examined for methanol extractable monomer content using gas chromatographic (GC)-mass spectrometry (MS). No detectable monomer was observed in any of the samples to a detection limit of 100 μg/mL.

Atomic Force Microscopy

The average plate roughness (R_a) and average peak-valley height (R_z) was determined via AFM, contact scanning mode. The two controls included the uncoated stainless steel and cured acrylic formulation with no additional phenyl acrylate derivative; both yielded R_z values of 0.819 μm. The R_a and R_z were determined for each formulation at varying concentrations of representative monomers (**3a**, **3b**, **3d**, **3e**, and **3f**). With the exception of **3a**, the smoothness as determined by the R_a and R_z generally increases as the concentration of the monomer increases owing to the increased dipole-dipole interactions of the coating (Table 2).

Comparing R_z of the cured coating formulations to the peak-valley requisite for surgical grade steel ($R_z \leq$ 1 μm, 320 grit, electropolished), several of the cured coating formulations were well within the requisite

Monomer	5 wt %	5 wt %	10 wt %	10 wt %	15 wt %	15 wt %	20 wt %	20 wt %
	R_z (μm)	R_a (μm)	R_z (μm)	R_a (μm)	R_z (μm)	R_a (μm)	R_z (μm)	R_a (μm)
3a	*0.7185*	0.1532	2.5917	0.1562	4.4568	0.1575	5.1233	0.1567
3b	2.265	0.1575	1.6857	0.1383	1.1517	0.107	*0.8888*	0.1077
3d	1.1553	0.1098	1.2905	0.1122	*0.7758*	0.1072	*0.6703*	0.105
3e	*0.785*	0.1532	1.3348	0.1552	*0.819*	0.1548	1.5117	0.1548
3f	1.4265	0.155	1.192	0.1545	*0.7897*	0.1537	*0.7102*	0.1528

Table 2. Surface Roughness Measured via AFM

Based on cantilever deflection values measured during the contact scanning mode.

R_z is the average peak-valley height of the cured coating. Values meeting minimum surgical grade steel requisites are italicized.

R_a is the average surface roughness of the cured coating.

See also Figure S1.

value for surgical grade steel with **3a** as a notable exception, providing evidence of smoothness capable of inhibiting many types of microbial growth by reducing the available surface area for attachment (Gillis and Gillis, 1996; Mei et al., 2011).

Biofilm Resistance Studies

Each bacterium (e.g., *E. coli*, *P. aeruginosa*, *S. aureus*, *Streptococcus pneumoniae*, and *Salmonella typhimurium*) was specifically chosen for its contribution to common infectious pathways including, but not limited to, food poisoning and life-threatening and/or nosocomial infections.

Having no halogenation, **3a** was utilized as an internal standard having no inherent biofilm-resistant structural component. For reference, we also compared the standard control coating (no compound **3**) to the uncoated portion of the slide. The motile bacteria examined (e.g., *E. coli.*, *P. aeruginosa*, and *S. typhimurium*) had nominal or increased biofilm development on the control coating, whereas the non-motile cocci had nominal or decreased biofilm development on the control coating relative to the uncoated portion of the slide. As exhibited via the aforementioned variable biofilm development, the control coating likely has limited biofilm inhibitory effect.

Overall (see Figures S2–S7), biofilm formation was observed on the uncoated portions and the levels of growth clearly fall over a wide spectrum. As a non-halogenated internal standard, **3a** did not exhibit any biofilm resistance. The monohalogenated derivatives (e.g., **3b**, **3c**, **3e**, and **3g**) showed some limited biofilm resistance especially at higher concentrations with **3e** resisting biofilm formation best. Dihalogenated monomers (**3d** and **3f**) seemed to impede biofilm formation better than their monohalogenated counterparts. Comparing chlorinated, brominated, and iodinated derivatives, the brominated monomers were the most effective biofilm-resistant monomers. Brominated coatings tended to perform better than chlorinated coatings with 40% of the brominated coatings passing our qualitative examination and 14% failing. Chlorinated coatings had a 15% pass rate with a 44% failure rate.

Laboratory conditions using lab-grown bacteria, which may have reduced immune functionality from multigenerational reproduction, may not provide an adequate environment for evaluating biofilm resistance. Therefore, we evaluated the coatings' biofilm resistance when exposed to 3.5 million gallons of raw clarified sewage for 2 days at the Abilene (Texas) Wastewater Reclamation Plant (see Figure S8). After preparing and evaluating the slides as before, the varying compositions' (**3a-g**) biofilm resistance produced comparatively consistent results to the previous bacterial studies (see Figure S8). Interestingly, visible algae growth was restricted solely to the BRApp (and not the slides) thereby indicating cursory resistance to algae growth.

To evaluate the monomers and concentrations for optimal biofilm resistance, all biofilm resistance data (single and multiple species biofilm resistance studies) were aggregated and normalized relative to the equivalent of no biofilm resistance differential between uncoated control and coating (Figure 1).

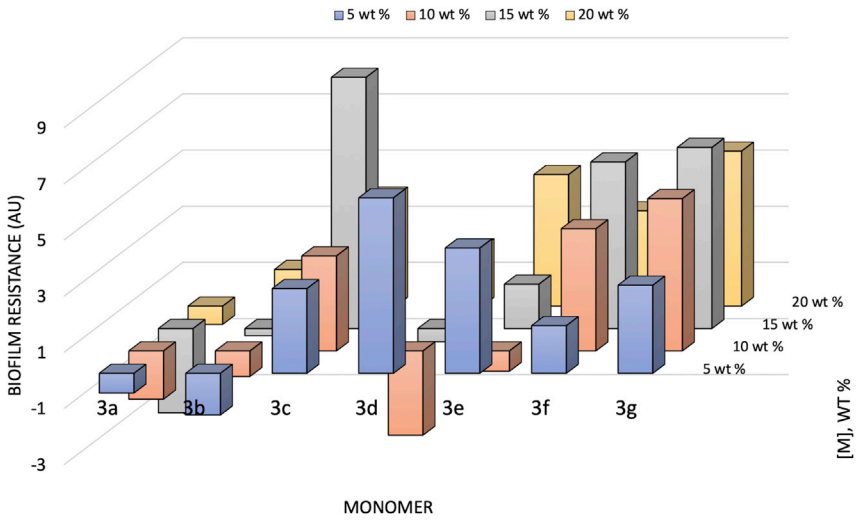

Figure 1. Normalized Quantitative Evaluation of Multiple Species Biofilm Resistance

Species evaluated include *E. coli*, *P. aeruginosa*, *S. aureus*, *S. pneumoniae*, and *S. typhimurium*.

Normalized relative to biofilm growth on control coating.

Reduced biofilm resistance relative to the control is negative.

Increased biofilm resistance relative to the control is positive.

See also Figures S2–S7.

In order to determine the most biofilm-resistant monomers, the normalized quantitative data seem to indicate that biofilm resistance is directly related to concentration of the monomers with the exception of the internal, non-halogenated control (**3a**). The normalized data demonstrate that **3b** is not biofilm resistant at the incorporated amounts in the coating. **3d** was more efficacious at lower concentrations indicating that the biostatic effect inherent to a MIC may be an important effect of biofilm resistance of this monomer. **3e** also exhibited a biostatic effect overall at low concentration; however, biofilm resistance generally increased with concentration. Both **3f** and **3g** were the most consistently biofilm resistant with increasing efficacy up to 15 weight percent. Furthermore, halogenation at the *para*-position seems to produce a stereotypic effect for enhanced biofilm resistance. Finally, the presence of softer halogens (e.g., bromine and iodine) on the monomers seems to result in increased biofilm resistance.

Surface Energy Analyses

Surface energy analyses may be accomplished via many methods; however, we chose a goniometric method for its simplicity and affordability. Using three fully characterized liquids to obtain statistical contact angle averages, the van Oss-Chaudhury-Good Equation 1 was solved linear algebraically for the following surface energy components: nonpolar (γ_s^{LW}), acid (γ_s^+), and base (γ_s^-) components (van Oss et al., 1987).

$$(1 + cos\theta_{sl})\gamma_l^{tot} = 2\left(\sqrt{\gamma_s^{LW}\gamma_l^{LW}} + \sqrt{\gamma_s^+\gamma_l^-} + \sqrt{\gamma_s^-\gamma_l^+}\right) \quad \text{(Equation 1)}$$

The polar component (γ_s^{AB}) and overall surface energy (γ_s) was then calculated via Equations 2 and 3, respectively (van Oss et al., 1988).

$$\gamma^{AB} = 2\sqrt{\gamma^+\gamma^-} \quad \text{(Equation 2)}$$

$$\gamma^{tot} = \gamma^{LW} + \gamma^{AB} \quad \text{(Equation 3)}$$

Table 3 tabulates the surface energy profiles for each polymerized phenyl acrylate derivative (**3a-g**, see Data S3 for homopolymer characterization).

In order to compare the surface energy profiles of the polymerized phenyl acrylate derivatives (**3a-g**), the surface energy profile was similarly obtained for collagen (insoluble and soluble), *S. aureus*, and *P. aeruginosa* (Table 4).

Substrate	γ_s	γ_s^{LW}	γ_s^{AB}	γ_s^+	γ_s^-
3a	35.14 ± 1.40	29.13 ± 1.20	6.01 ± 0.80	1.93 ± 0.50	6.51 ± 1.46
3b[a]	41.44 ± 1.11	36.41 ± 0.70	5.04 ± 1.57	0.198 ± 0.077	51.39 ± 1.11
3c	28.46 ± 0.67	25.64 ± 0.67	2.83 ± 0.60	2.73 ± 0.61	1.31 ± 0.43
3d	39.08 ± 2.44	29.62 ± 0.63	9.46 ± 2.14	0.736 ± 0.230	32.47 ± 4.41
3e	29.91 ± 0.70	24.41 ± 0.46	5.50 ± 0.27	0.745 ± 0.043	10.22 ± 0.61
3f	36.06 ± 1.62	26.94 ± 0.56	9.12 ± 1.50	4.26 ± 0.91	9.70 ± 2.05
3g	34.48 ± 0.43	33.15 ± 0.39	1.33 ± 0.28	1.15 ± 0.24	0.485 ± 0.130

Table 3. Surface Energy Profile of Derivatized Phenyl Acrylate Polymers

All units are mJ/m^2 ± SEM where number of samples (*N*) is 36 (**3a**), 24 (**3b**), 18 (**3c**), 18 (**3d**), 24 (**3e**), 36 (**3f**), and 18 (**3g**). See Transparent Methods. Calculations based on contact angles from bromonaphthalene, formamide, and water.

[a]Obtaining a smooth coating without smearing or orange peeling was difficult and may have contributed to an anomalous/inaccurate surface energy profile; however, for completeness, the surface energy profile for **3b** was included in the dataset.

The surface energy component values for soluble collagen (e.g., γ_s^{LW}, γ_s^{AB}, and γ_s) were slightly higher than established literature values with additional values for the acid (γ_s^+) and base (γ_s^-) components (Lewandowska et al., 2016; Skopińska-Wiśniewska et al., 2009). Insoluble collagen is noticeably differentiated from the soluble collagen per the base (γ_s^-) components illustrating an increased substrate dipole for the soluble collagen. Often a quick comparison of the overall surface energy (γ_s) of two interacting materials has been used to establish a degree of interfacial interaction between two materials.

Based on the previous literature relating compositional variations to contact angles, the surface energy values for phenyl acrylate homopolymers could be inferred to impact the surface chemistry of copolymer formulations (Cassie, 1948; Drelich et al., 1996). In order to directly compare the surface energies of the phenyl acrylic coatings with collagen and select bacteria, the overall surface energy (γ_s) of each was plotted; however, no clear trend is apparent (Figure 2).

Therefore, each individual component was examined for all phenyl acrylate monomer derivatives, collagens, and bacteria. The most interesting individual component comparisons involved the polar (γ_s^{AB}) and base components (γ_s^-) plotted in Figures 3 and 4, respectively.

Excepting **3a** (internal control) and **3b** (inaccurate profile), the substrates with the most similar γ_s^{AB} include **3d**, **3e**, **3f**, insoluble collagen, *P. aeruginosa*, and *S. aureus*. Focusing on the **3d**, **3e**, **3f**, and bacteria, the similarities in the polar component (γ_s^{AB}) likely indicates a more significant thermodynamic interaction. The single species biofilm resistance studies seem to qualitatively support a more significant interaction between **3d**, **3e**, **3f**, and bacteria. The low γ_s^{AB} values for both **3c** and **3g** likely result in reduced polar interactions explaining the observed biofilm resistance.

Substrate	γ_s	γ_s^{LW}	γ_s^{AB}	γ_s^+	γ_s^-
Collagen, insoluble[a]	45.75 ± 0.83	40.08 ± 0.46	5.67 ± 0.75	1.51 ± 0.39	6.90 ± 1.52
Collagen, soluble[b]	37.08 ± 2.15	30.13 ± 1.22	6.95 ± 1.70	0.806 ± 0.26	16.08 ± 3.99
S. aureus[c]	43.91 ± 0.50	39.63 ± 0.37	4.29 ± 0.49	0.066 ± 0.014	73.54 ± 0.69
P. aeruginosa[c]	39.26 ± 0.77	34.82 ± 0.46	4.44 ± 0.78	0.089 ± 0.029	69.07 ± 1.99

Table 4. Surface Energy Profile of Various Biologic Materials

All units are mJ/m^2 ± SEM where number of samples (*N*) is 18 (collagen, insoluble), 36 (collagen, soluble), 21 (*S. aureus*), and 18 (*P. aeruginosa*). See Transparent Methods.

[a]Calculations based on contact angles from bromonaphthalene, formamide, and water for insoluble collagen (100 μg/mL).

[b]Calculations based on contact angles from bromonaphthalene, formamide, and water for soluble collagen (100 μg/mL) in phosphate buffer solution (1x, pH = 7.4).

[c]Calculations based on contact angles from bromonaphthalene, dimethylsulfoxide, and water.

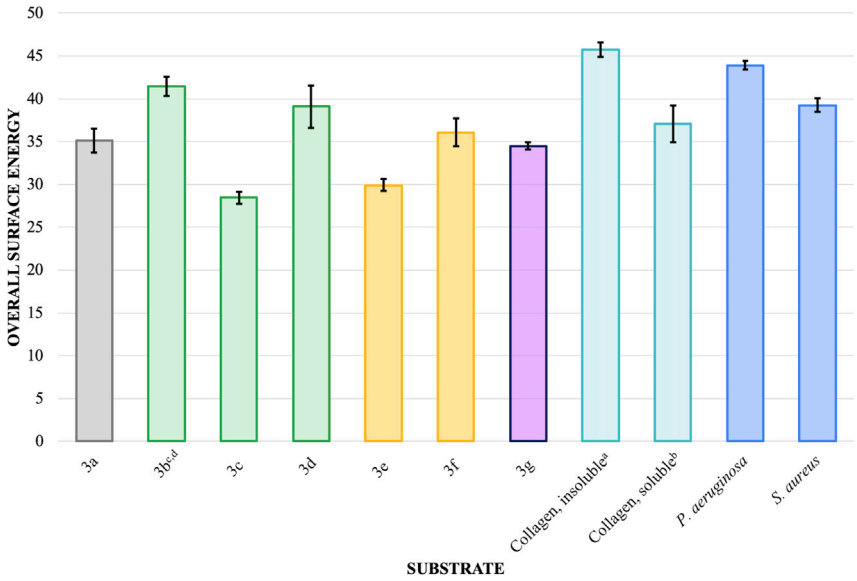

Figure 2. Overall Surface Energy Comparison (γ_s) of Phenyl Acrylic Coatings, Collagens, and Bacteria

All units are mJ/m^2 ± SEM where number of samples (*N*) is 36 (**3a**), 24 (**3b**), 18 (**3c**), 18 (**3d**), 24 (**3e**), 36 (**3f**), 18 (**3g**), 18 (collagen, insoluble), 36 (collagen, soluble), 21 (*S. aureus*), and 18 (*P. aeruginosa*). See Transparent Methods.

[a]Calculations based on contact angles from bromonaphthalene, formamide, and water for insoluble collagen (100 μg/mL).

[b]Calculations based on contact angles from bromonaphthalene, formamide, and water for soluble collagen (100 μg/mL) in phosphate buffer solution (1x, pH = 7.4).

[c]Calculations based on contact angles from bromonaphthalene, dimethylsulfoxide, and water.

[d]Obtaining a smooth coating without smearing or orange peeling was difficult and may have contributed to an anomalous/inaccurate surface energy profile; however, for completeness, the surface energy profile for **3b** was included in the dataset.

Because the magnitude of the acid components (γ_s^+) is comparatively small for most monomers, the base components (γ_s^-) shown in Figure 4 should be the most significant interaction.

3d is qualitatively less efficacious as a biofilm-resistant substrate perhaps owing to the larger nonpolar component, which may obfuscate the relatively hard (i.e., charge dense) chlorine atoms, especially when bound in an amorphous, cross-linked polymer matrix with little polar directionality. Furthermore, biofilm formation also seems to be more significantly inhibited by the softer halogens (e.g., bromine and iodine).

Based on Figures 1, **3c**, **3e**, **3f**, and **3g** were clearly the most biofilm-resistant substrates examined in this study with limited efficacy of **3d**. Based on Figure 3, biofilm resistance of **3c** and **3g** have reduced polar components (γ_s^{AB}) and thus limited polar interactions with bacteria and adhesins. Figure 4 shows **3d**, **3e**, and **3f** having appreciable base components (γ_s^-). A significant intermolecular (base-base) repulsion may be a causative agent of biofilm resistance for monomers with significantly large base components (γ_s^-). *S. aureus*, a non-motile bacterium, was most affected by **3c** and **3g**, whereas both **3e** and **3f** equally inhibited biofilm formation of the motile *P. aeruginosa*. With surface interactions being diffusion controlled, *S. aureus* adhesion is thermodynamically controlled. The parallel movement of *P. aeruginosa* along a surface interface would contribute a competing kinetic effect to the thermodynamic driving force for surface adhesion. Owing to kinetic competition, the biofilm resistance of **3e** and **3f** is slightly diminished for *P. aeruginosa* relative to *S. aureus* as observed.

The increased thermodynamic biofilm resistance may be 2-fold. First, as previously stated, polar interactions of the bacterium with the monomers contribute significantly to adhesion thereto. Diminished polar surface energy components of the substrate reduce the adhesive propensity for bacteria to bind to a substrate. Conversely, interacting base components (γ_s^-) of a stationary substrate with a diffusing bacterium would have an increasing intermolecular charge repulsion as the distance between substrate and bacterium decreases. Such would especially be present in the non-chelated N2 domain of the surface protein

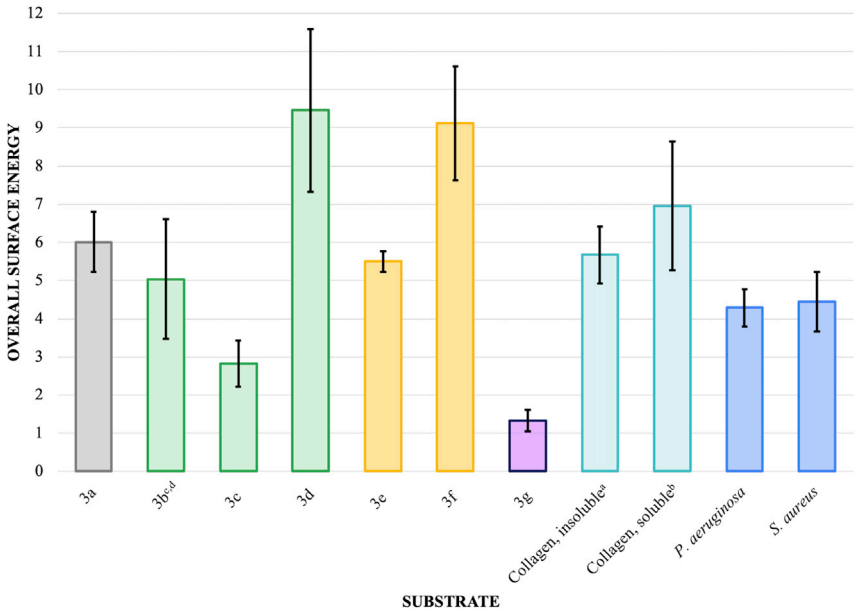

Figure 3. Surface Energy Polar Component (γ_s^{AB}) Comparison of Phenyl Acrylic Coatings, Collagens, and Bacteria

All units are mJ/m^2 ± SEM where number of samples (*N*) is 36 (**3a**), 24 (**3b**), 18 (**3c**), 18 (**3d**), 24 (**3e**), 36 (**3f**), 18 (**3g**), 18 (collagen, insoluble), 36 (collagen, soluble), 21 (*S. aureus*), and 18 (*P. aeruginosa*). See Transparent Methods.

[a]Calculations based on contact angles from bromonaphthalene, formamide, and water for insoluble collagen (100 μg/mL).

[b]Calculations based on contact angles from bromonaphthalene, formamide, and water for soluble collagen (100 μg/mL) in phosphate buffer solution (1x, pH = 7.4).

[c]Calculations based on contact angles from bromonaphthalene, dimethylsulfoxide, and water.

[d]Obtaining a smooth coating without smearing or orange peeling was difficult and may have contributed to an anomalous/inaccurate surface energy profile; however, for completeness, the surface energy profile for **3b** was included in the dataset.

SdrC of *S. aureus* (Pi et al., 2020). Second and likely to a lesser degree, a polarizable soft atom (e.g., bromine or iodine) or other polarizable moiety could allow the bacterium to remain associated with the substrate in the absence of reversible adhesion during primary colonization. The latter reasoning is used to explain, in part, limited bacterial attachment onto superhydrophilic substrates (Noorisafa et al., 2016; Yuan et al., 2017).

Conclusions

Seven monomers (i.e., phenyl acrylate and halogenated derivatives thereof) were successfully synthesized through a standard laboratory synthesis. Each monomer was added at variable concentrations (e.g., 5, 10, 15, and 20 weight percent) to a compatible industrial formulation that was subsequently UV cured onto various substrates. Examination via AFM illustrated that several of the cured coating formulations, including those of **3e** and **3f**, yielded exceptionally smooth coatings with limited surface areas evidenced by average peak to valley heights (R_z) less than 1.0 μm and very low roughness (R_a) measurements. **3f** exhibited an inverse relationship of both R_z and R_a as concentration increased. The coatings were then analyzed for single (e.g., *E. coli*, *P. aeruginosa*, *S. aureus*, *S. pneumoniae*, and *S. typhimurium*) and multiple (e.g., clarified raw sewage) species biofilm resistance. After normalizing the biofilm resistance studies, coatings incorporating the brominated phenyl acrylate monomers (e.g., **3e** and **3f**), the monochlorinated **3c**, and the monoiodinated **3g** exhibited significant biofilm resistance. Because biofilm resistance is a symbiotic, multi-determinant system involving the physical and chemical interaction of both substrate and bacteria, we also examined the surface energies of the polymerized phenyl acrylate derivatives, collagen, and two representative bacteria (e.g., *P. aeruginosa* and *S. aureus*). Comparative analysis of each surface energy component demonstrated that the polar component (γ_s^{AB}) is likely the primary thermodynamic contributor to the observed biofilm resistance. Small polar components of the substrate reduce the adhesiveness of bacteria to the substrate, whereas a large base component (γ_s^-) repels the bacterium.

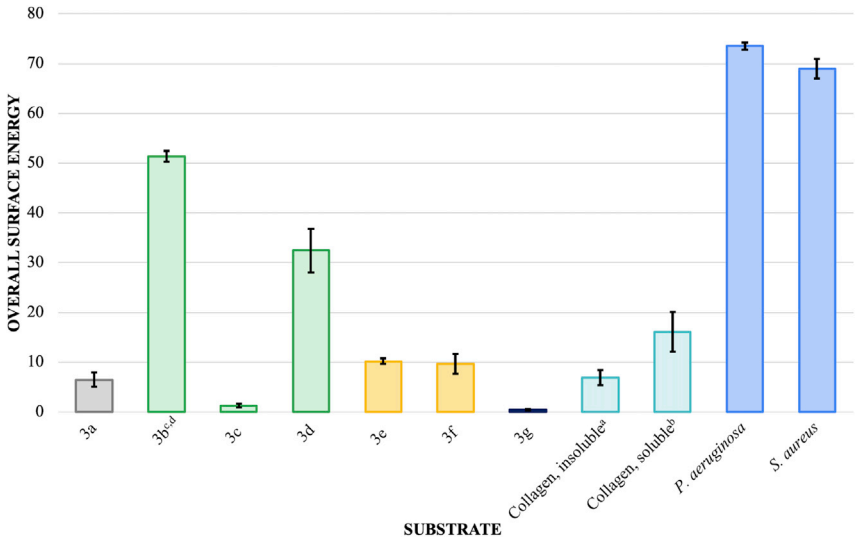

Figure 4. Surface Energy Base Component (γ_s^-) Comparison of Phenyl Acrylic Coatings, Collagens, and Bacteria

All units are mJ/m^2 ± SEM where number of samples (*N*) is 36 (**3a**), 24 (**3b**), 18 (**3c**), 18 (**3d**), 24 (**3e**), 36 (**3f**), 18 (**3g**), 18 (collagen, insoluble), 36 (collagen, soluble), 21 (*S. aureus*), and 18 (*P. aeruginosa*). See Transparent Methods.

[a]Calculations based on contact angles from bromonaphthalene, formamide, and water for insoluble collagen (100 μg/mL).

[b]Calculations based on contact angles from bromonaphthalene, formamide, and water for soluble collagen (100 μg/mL) in phosphate buffer solution (1x, pH = 7.4).

[c]Calculations based on contact angles from bromonaphthalene, dimethylsulfoxide, and water.

[d]Obtaining a smooth coating without smearing or orange peeling was difficult and may have contributed to an anomalous/inaccurate surface energy profile; however, for completeness, the surface energy profile for **3b** was included in the dataset.

Repulsive intermolecular interactions between base components of both the substrate and bacteria prevent intimate bacterial association with the substrate. Secondarily, we posit that the presence of soft atoms (e.g., bromine and iodine) and/or polarizable moieties in the coating may allow bacterial association while inhibiting adhesion and biofilm formation during primary colonization.

Limitations of the Study

Potential caveats of this published work could include the following. First, as mentioned in the text, our fundamental assumption throughout our biological experimentation is that biofilm growth cannot occur without primary colonization. Although we are not explicitly studying primary colonization, we are examining the results of microbial colonization that are possible only if primary colonization occurs via a significant substrate-bacteria interfacial interaction, an interaction that is limited in the latter stages of biofilm growth. Also because we used non-virulent bacterial strains for researcher safety, biofilm formation and resistance thereto may differ from virulent strains of the same species. Finally, goniometric surface energy analyses, like those reported herein, have been shown to differ from other surface energy analyses that do not use contact angle measurements (e.g., density functional theory [DFT] and cleaving method); however, the non-contact angle methods are most effectively implemented with well-defined structures unlike those examined herein (Tran et al., 2016; Gilman, 1960; Jaccodine, 1963).

Resource Availability

Lead Contact

Further information and requests related to the research published herein should be directed to and fulfilled by the Lead Contact, T. Brian Cavitt (tbcavitt@lipscomb.edu).

Materials Availability

All unique/stable reagents generated in this study are available on request from the Lead Contact but may require a payment and/or Materials Transfer Agreement if there is potential for commercial application.

Data and Code Availability

The published article includes all datasets generated or analyzed during this study.

METHODS

All methods can be found in the accompanying Transparent Methods supplemental file.

SUPPLEMENTAL INFORMATION

Supplemental Information can be found online at https://doi.org/10.1016/j.isci.2020.101702.

ACKNOWLEDGMENTS

The authors would like to thank the Albemarle Corporation for providing DMPA and Allied Photochemical for providing the standard industrial formulation used. We would also like to gratefully acknowledge the financial support of The Welch Foundation (Grant R-0021), the Abilene Christian University Office of Research and Sponsored Programs, and Lipscomb University's Office of the Provost and Department of Chemistry and Biochemistry.

AUTHOR CONTRIBUTIONS

Conceptualization, T.B.C.; Methodology, T.B.C., J.G.C., R.A.F., C.J.H., J.R.L., D.S.O., and D.S.; Validation, T.B.C.; Formal Analysis, T.B.C., J.G.C., V.N.G., D.S.O., and P.R.P.; Investigation, J.G.C., A.R.D., R.A.F., T.C.G., V.N.G., P.R.H., E.B.H., C.J.H., J.R.L., J.A.L., D.S.O., P.R.P., D.S., and W.W.; Resources, T.B.C.; Data Curation, T.B.C., J.G.C., V.N.G., D.S.O., and P.R.P.; Writing – Original Draft, T.B.C.; Writing – Review & Editing, T.B.C.; Visualization, T.B.C.; Supervision, T.B.C.; Project Administration, T.B.C.; Funding Acquisition, T.B.C.

DECLARATION OF INTERESTS

The Lead Contact and a coauthor have two patents related to the research herein (Cavitt and Faulkner, 2015, 2017). The authors declare no other competing interest.

Received: May 26, 2020
Revised: August 3, 2020
Accepted: October 15, 2020
Published: November 20, 2020

REFERENCES

Abbott, A., Abel, P.D., Arnold, D.W., and Milne, A. (2000). Cost-benefit analysis of the use of TBT: the case for a treatment approach. Sci. Total. Environ. *258*, 5–19.

Bhatt, L., Chen, L., Guo, J., Klie, R.F., Shi, J., and Pesavento, R.P. (2020). Hydrolyzed Ce(IV) salts limit sucrose-dependent biofilm formation by Streptococcus mutans. J. Inorg. Biochem. *206*, 110997.

Cassie, A.B.D. (1948). Contact angles. Discuss. Faraday Soc. *3*, 11–16.

Cleaveland, P. (2005). An evolution in coatings. Med. Des. Technol. *6*, 18–22.

Cavitt, T.B. and Faulkner, R.A.H. (2015). Biofilm resistant polymer materials. U.S. Patent No.: 9,072,292 B2.

Cavitt, T.B. and Faulkner, R.A.H. (2017). Biofilm resistant polymer materials. U.S. Patent No.: 9,591,848 B2.

Conrad, J.C., and Poling-Skutvik, R. (2018). Confined flow: consequences and implications for bacteria and biofilms. Annu. Rev. Chem. Biomol. Eng. *9*, 175–200.

Cooney, J.J., and Tang, R.J. (1999). Quantifying effects of antifouling paints on microbial biofilm formation. Methods Enzymol. *310*, 637–644.

Deng, J., Molaei, M., Chisholm, N.G., and Stebe, K.J. (2020). Motile bacteria at oil-water interfaces: *Pseudomonas aeruginosa*. Langmuir *36*, 6888–6902.

Drelich, J., Wilbur, J.L., Miller, J.D., and Whitesides, G.M. (1996). Contact angles for liquid drops at a model heterogeneous surface consisting of alternating and parallel hydrophobic/hydrophilic strips. Langmuir *12*, 1913–1922.

Flemming, H.–C. (2002). Biofouling in water systems–cases, causes and countermeasures. Appl. Microbiol. Biotechnol. *59*, 629–640.

Gillis, R.J., and Gillis, J.R. (1996). A comparative study of bacterial attachment to high-purity water system surfaces. Ultrapure Water *13*, 27–36.

Gilman, J.J. (1960). Direct measurements of the surface energies of crystals. J. Appl. Phys. *31*, 2208–2218.

Iwamoto, K. and Matsutomo, S. (2018). Biofilm amount determination method and a water treatment system comprising filtration membrane module. Japan Patent No.: 2018-202338 A.

Jaccodine, R.J. (1963). Surface energy of germanium and silicon. J. Electrochem. Soc. *110*, 524–527.

Kandiyote, N.S., Avisdris, T., Arnusch, C.J., and Kasher, R. (2019). Grafted polymer coatings enhance fouling inhibition by an antimicrobial peptide on reverse osmosis membranes. Langmuir *35*, 1935–1943.

Kenawy, el-R., Worley, S.D., and Broughton, R. (2007). The chemistry and applications of antimicrobial polymers: a state-of-the-art review. Biomacromolecules *8*, 1359–1384.

Kõljalg, S., Smidt, I., Chakrabarti, A., Bosscher, D., and Mändar, R. (2020). Exploration of singular and synergistic effect on xylitol and erythritol on

causative agents of dental caries. Sci. Rep. *10*, 6297–6304.

Lewandowska, K., Sionkowska, A., Grabska, S., and Kaczmarek, B. (2016). Surface and thermal properties of collagen/hyaluronic acid blends containing chitosan. Int. J. Bio. Macromol *92*, 371–376.

Li, C., Jiang, C., Jing, H., Jiang, C., Wang, H., Du, X., and Lou, Z. (2020). Separation of phenolics from peony flowers and their inhibitory activities and action mechanism on bacterial biofilm. Appl. Microbiol. Biotechnol. *104*, 4321–4332.

Lu, S., Zhang, Z., Xu, Y., Lu, J., Tang, W., and Zhang, J. (2020). Effect of new carbonyl cyanide aromatic hydrazones on biofilm inhibition against methicillin resistant *Staphylococcus aureus*. RSC Adv. *10*, 17854–17861.

McLay, R.B., Nguyen, H.N., Jaimes-Lizcano, Y.A., Dewangan, N.K., Alexandrova, S., Rodrigues, D.F., Cirino, P.C., and Conrad, J.C. (2018). Level of fimbriation alters the adhesion of *Escherichia coli* bacteria to interfaces. Langmuir *34*, 1133–1142.

Mei, L., Busscher, H.J., Mei, H.C.V.D., and Ren, Y. (2011). Influence of surface roughness on streptococcal adhesion forces to composite resins. Dent. Mater. *27*, 770–778.

Monroe, D. (2007). Looking for chinks in the armor of bacterial biofilms. PLoS Biol. *5*, 2458–2461.

Moola, A.K., Balasubramanni, S., Nithya, C., and Diana, R.K.B. (2019). Preparation, characterization of silver-nanoparticles from seed coat exudates of celastrus paniculatus willd and their bactericidal and biofilm inhibition effects. Int. J. Pharm. Sci. Drug Res. *11* (5), 164–173.

Montanaro, L., Campoccia, D., Pirini, V., Ravaioli, S., and Otto, M. (2007). Antibiotic multiresistance strictly associated with IS256 and ica genes in *Staphylococcus epidermidis* strains from implant orthopedic infections. J. Biomed. Mater. Res. A *83*, 813–818.

Namasivayam, S.K.R., Francis, A.L., Bharani, R.S.A., and Nachiyar, C.V. (2019). Bacterial biofilm or biofouling networks with numerous resilience factors from real water supplies of Chennai and their enhanced susceptibility to biocomposite nanoparticles. J. Clean. Prod. *231*, 872–898.

Namivandi-Zangeneh, R., Yang, Y., Xu, S., Wong, E.H.H., and Boyer, C. (2020). Antibiofilm platform based on the combination of antimicrobial polymers and essential oils. Biomacromolecules *21*, 262–272.

Noorisafa, F., Razmjou, A., Emami, N., Low, Z.-X., Korayem, A.H., and Kajani, A.A. (2016). Surface modification of polyurethane via creating a biocompatible superhydrophilic nanostructured layer: role of surface chemistry and structure. J. Exp. Nanosci. *11*, 1087–1109.

O'Flaherty, S., Ross, R.P., Meanry, W., and Fitzgerald, G.F. (2004). Potential of the polyvalent anti-staphylococcus bacteriophage K for control of antibiotic-resistant staphylococci from hospitals. Appl. Environ. Microbiol. *1*, 1836–1842.

Pi, Y., Chen, W., and Ji, Q. (2020). Structural basis of *Staphylococcus aureus* surface protein SdrC. Biochemistry *59*, 1465–1469.

Pickens, S.R. (2009). Method for inhibiting biofilm growth. US patent application Publication: US 2009/018062 A1.

Skopińska-Wiśniewska, J., Sionkowska, A., Kaminska, A., Kazinica, A., Jachimiak, R., and Drewa, T. (2009). Surface properties of collagen/elastin based biomaterials for tissue regeneration. Appl. Surf. Sci. *225*, 8286–8292.

Tran, R., Xu, Z., Radhakrishnan, B., Winston, D., Sun, W., Persson, K.A., and Ong, S.P. (2016). Surface energies of elemental crystals. Sci. Data *3*, 160080.

Valarikova, J., Cizova, A., Rackova, L., and Bystricky, S. (2020). Anti-staphylococcal activity of quaternized mannan from the yeast *Candida albicans*. Carbohydr. Polym. *240*, 116288.

van Oss, C.J., Chaudhury, M.K., and Good, R.J. (1987). Monopolar surfaces. Adv. Colloid Interf. Sci. *28*, 35–64.

van Oss, C.J., Good, R.J., and Chaudhury, M.K. (1988). Additive and nonadditive surface tension components and the interpretation of contact angles. Langmuir *4*, 884–891.

Vertes, A., Hitchins, V., and Phillips, K.S. (2012). Analytical challenges of microbial biofilms on medical devices. Anal. Chem. *84*, 3858–3866.

Vissers, T., Koumakis, N., Hermes, M., Brown, A.T., Schwarz-Linek, J., Dawson, A., and Poon, W.C.K. (2019). Dynamical analysis of bacteria in microscopy movies. PLoS One *14*, 1–15.

Yuan, Y., Hays, M.P., Hardwidge, P.R., and Kim, J. (2017). Surface characteristics influencing bacterial adhesion to polymeric substrates. RSC Adv. *7*, 14254–14261.

iScience, Volume *23*

Supplemental Information

Thermodynamic Surface Analyses to Inform Biofilm Resistance

T. Brian Cavitt, Jasmine G. Carlisle, Alexandra R. Dodds, Rebecca A. Faulkner, Tyson C. Garfield, Verena N. Ghebranious, Phillip R. Hendley, Emily B. Henry, Charles J. Holt, Jordan R. Lowe, Jacob A. Lowry, D. Spencer Oskin, Pooja R. Patel, Devin Smith, and Wenting Wei

SUPPLEMENTAL INFORMATION

Data S1. Spectra of Products: Related to Table 1.

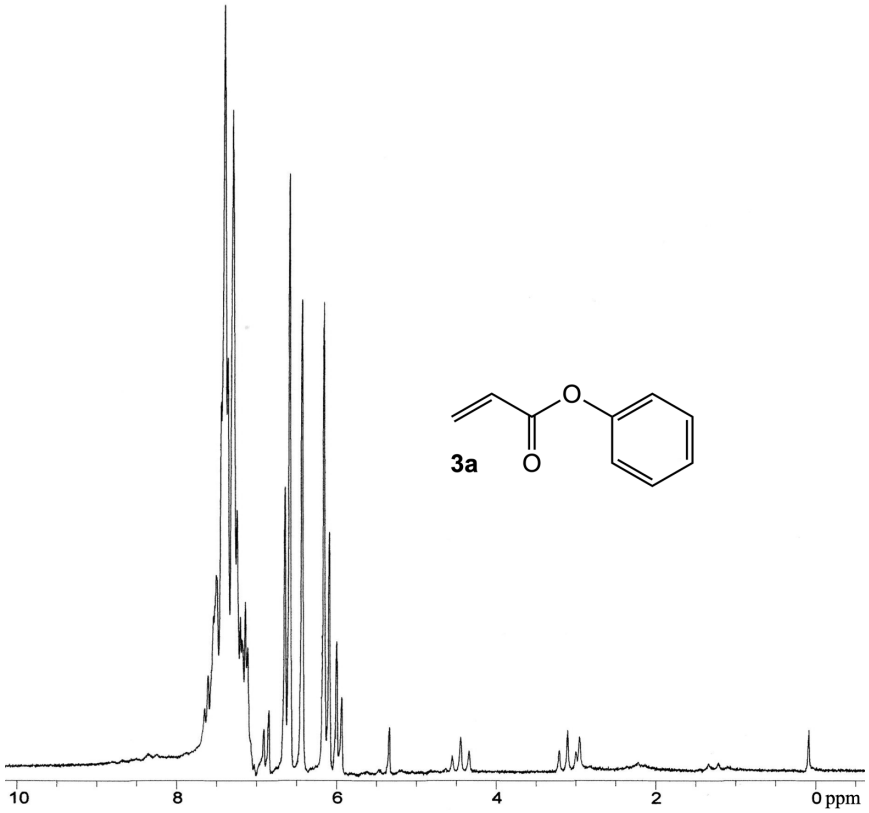

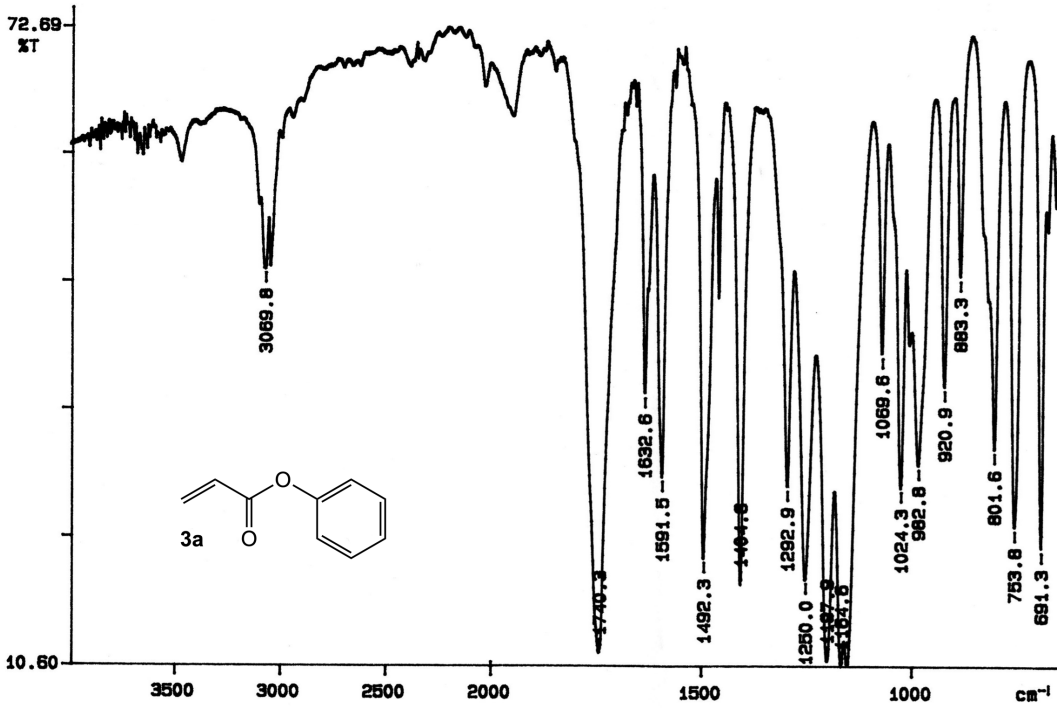

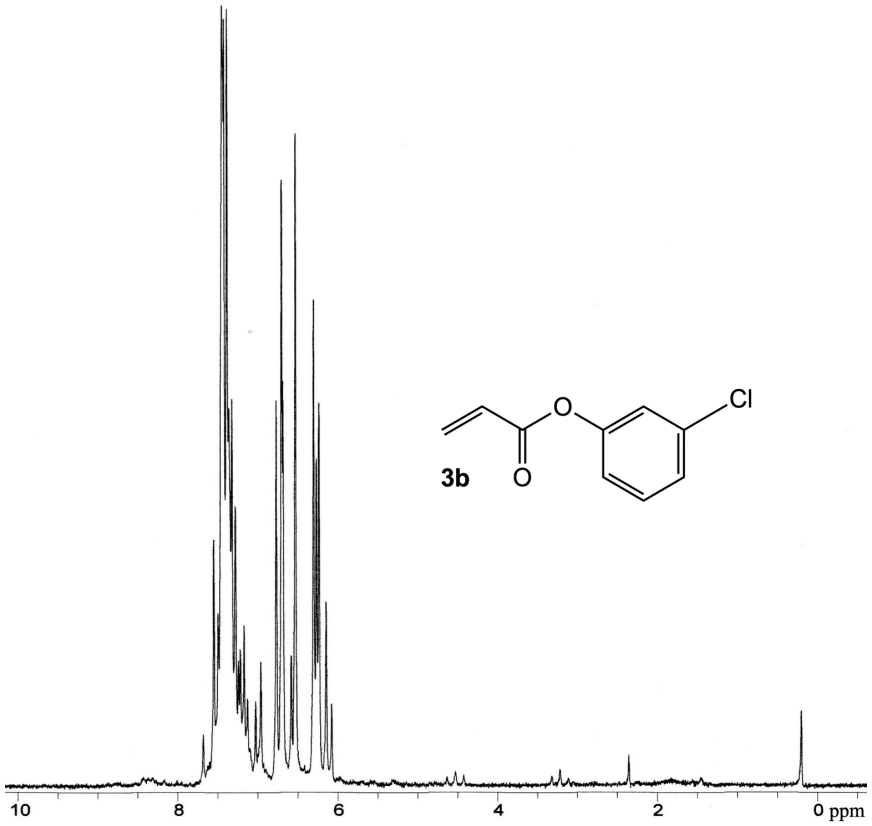
Cl
O
O
3b
10
8
6
4
2
0 ppm

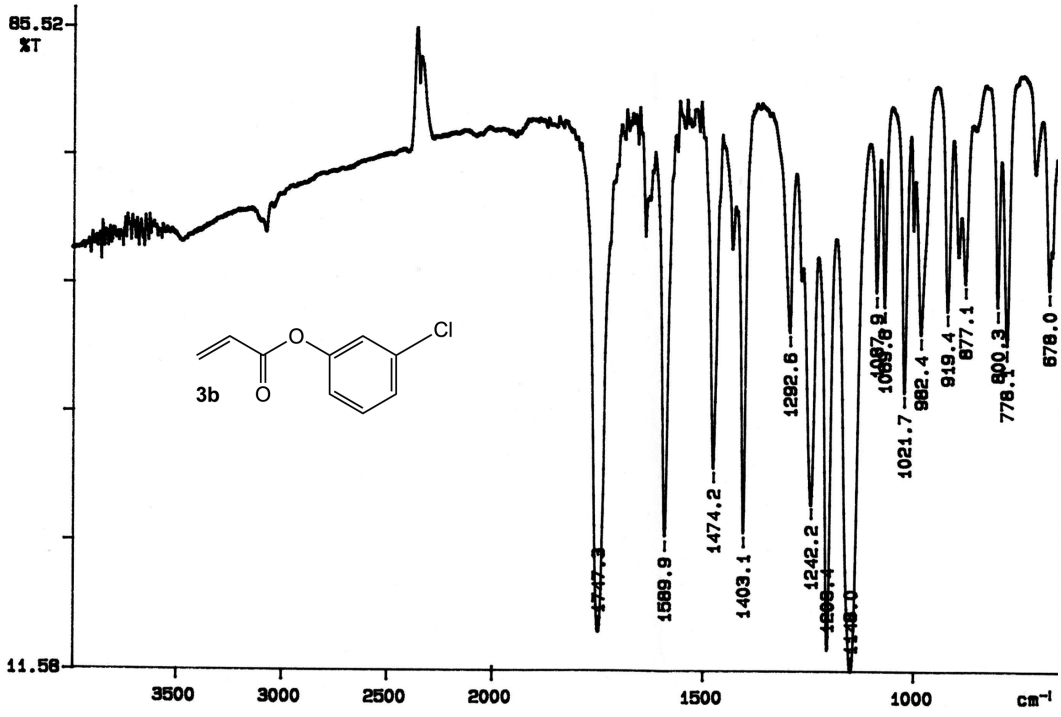
85.52
%T
11.58
Cl
O
O
3b
1589.9
1474.2
1403.1
1292.6
1242.2
1021.7
982.4
919.4
877.1
778.1
678.0
3500
3000
2500
2000
1500
1000
cm-1

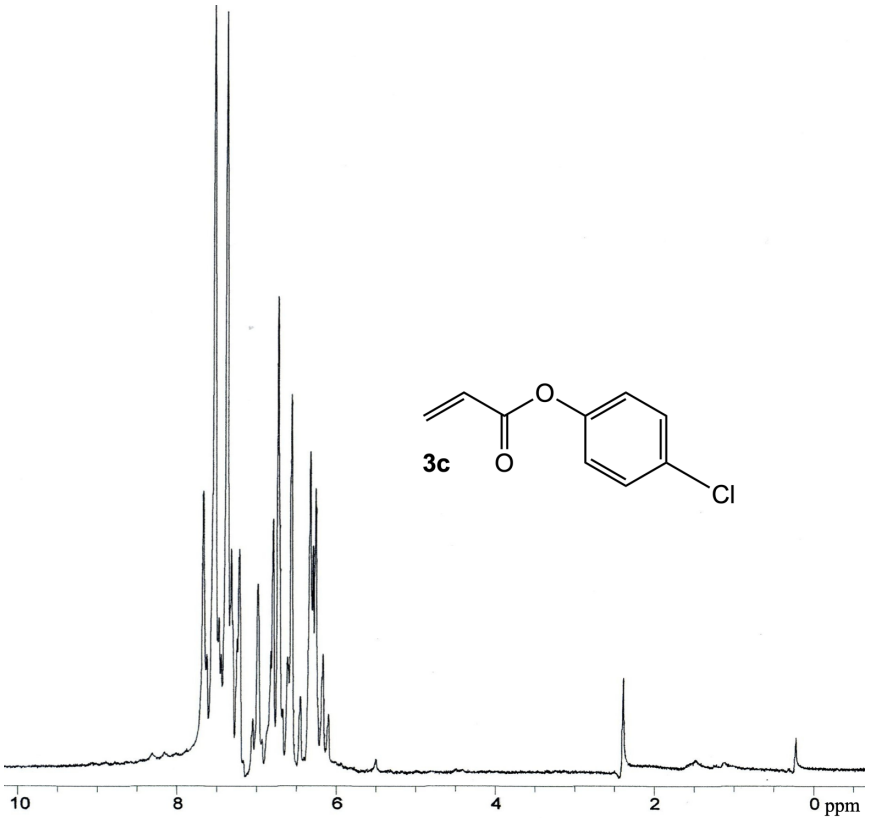
3c
O
O
Cl
10
8
6
4
2
0 ppm

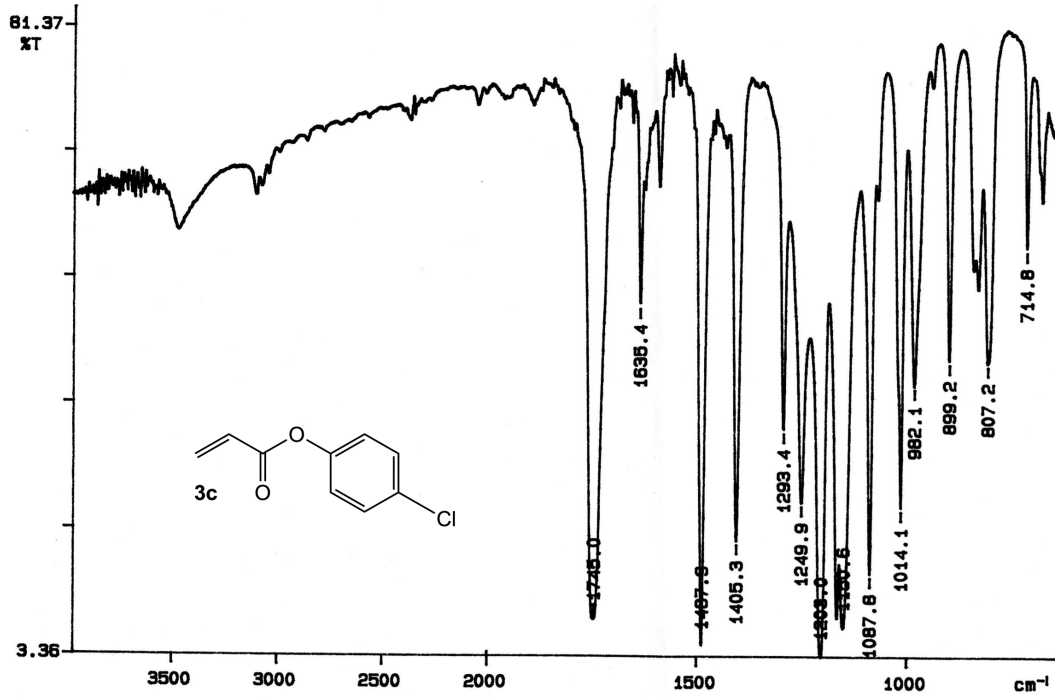
81.37
%T
3.36
3c
O
O
Cl
1635.4
1405.3
1293.4
1249.9
1014.1
982.1
899.2
807.2
714.8
3500
3000
2500
2000
1500
1000
cm⁻¹

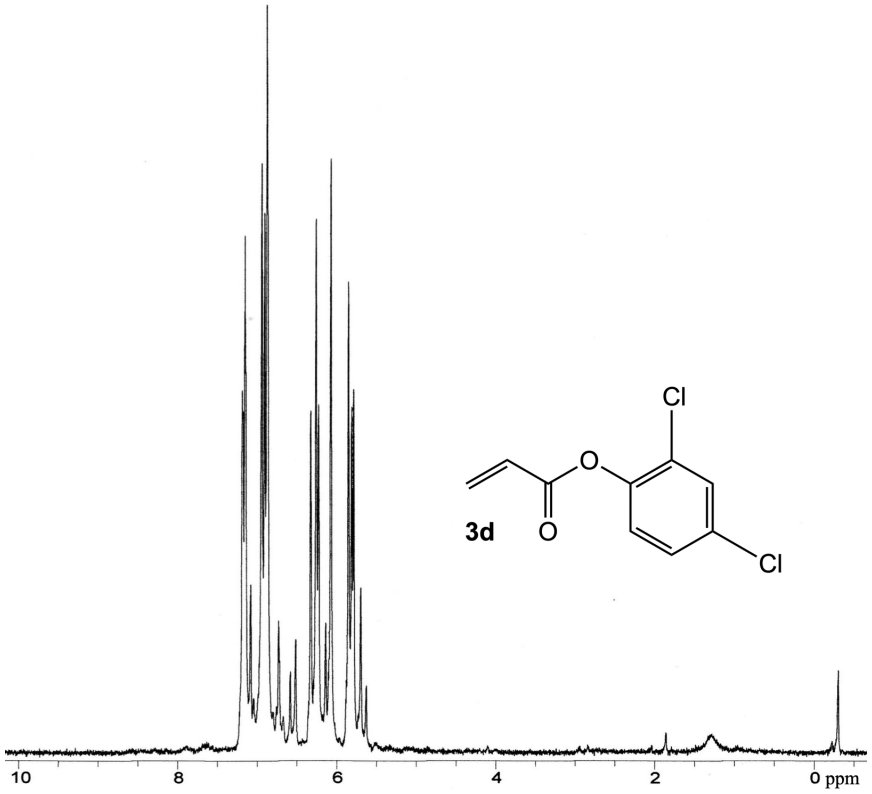
Cl
O
O
3d
Cl
10
8
6
4
2
0 ppm

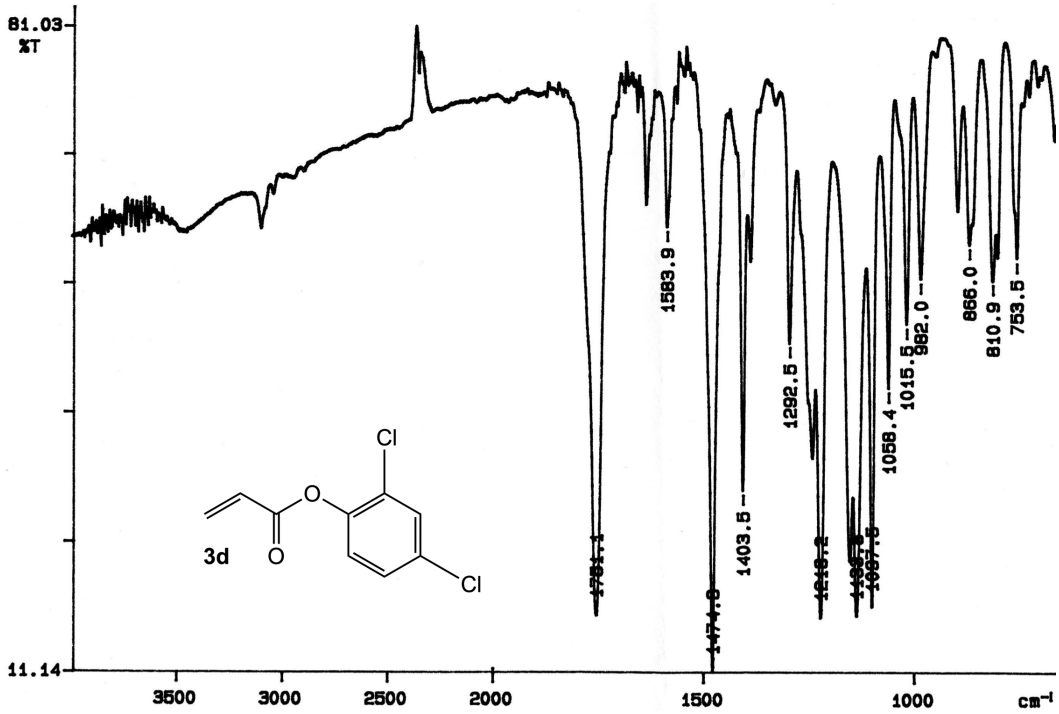
81.03
%T
11.14
1583.9
1403.5
1292.5
1058.4
1015.5
982.0
866.0
810.9
753.5
Cl
O
O
3d
Cl
3500
3000
2500
2000
1500
1000
cm-1

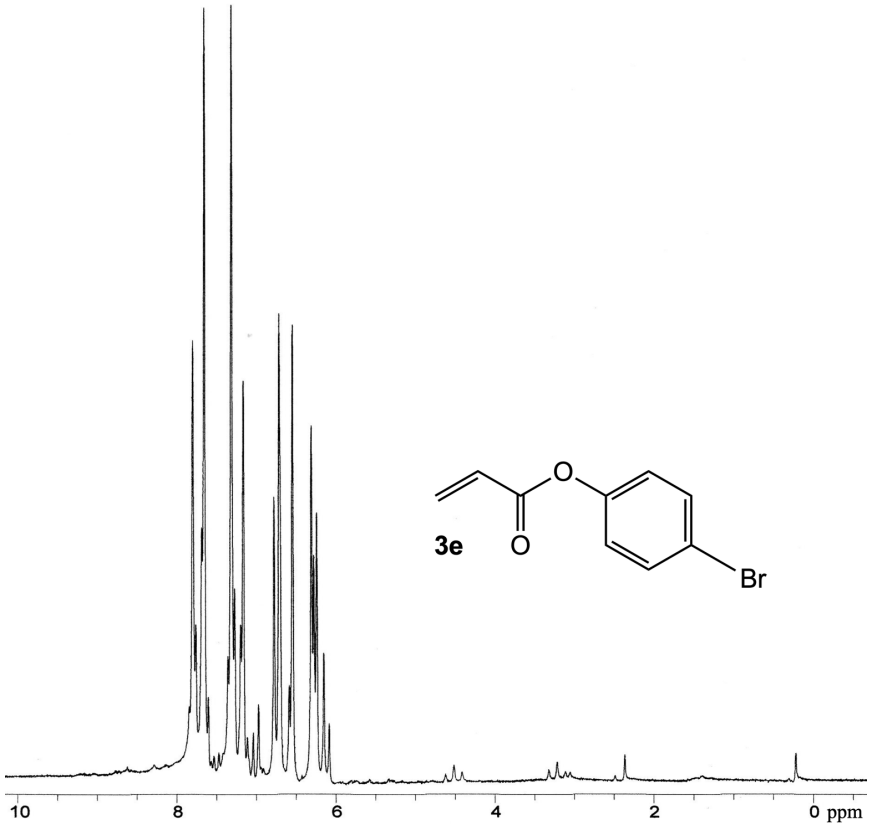
3e
O
O
Br
10
8
6
4
2
0 ppm

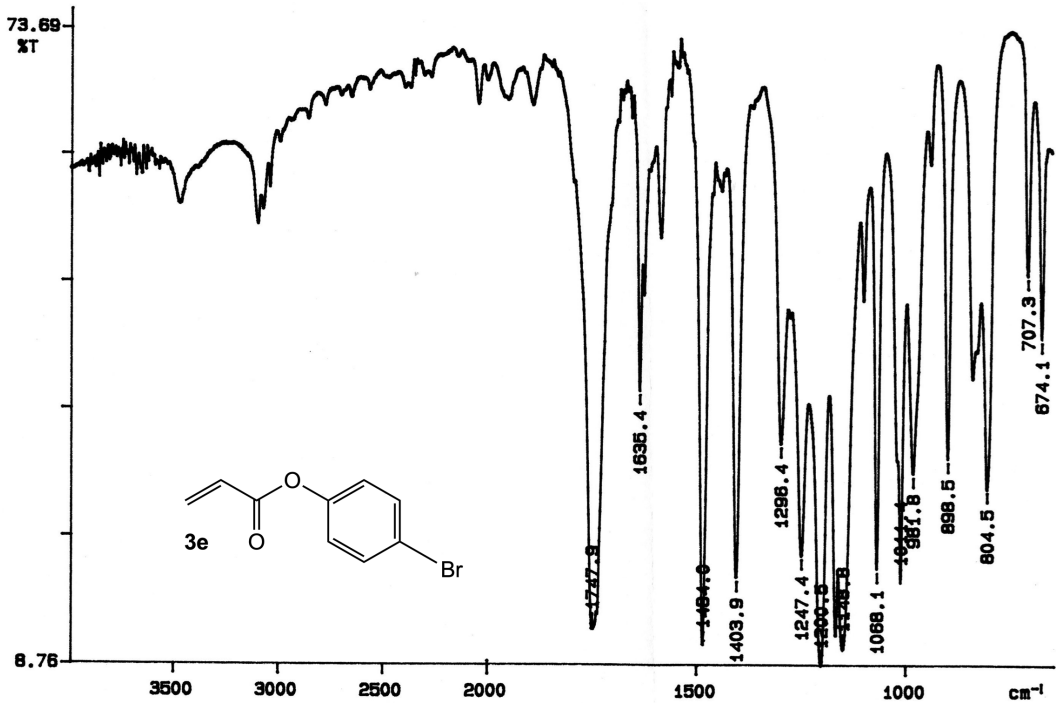
73.69
%T
8.76
3e
O
O
Br
1635.4
1403.9
1298.4
1247.4
1068.1
898.5
804.5
707.3
674.1
3500
3000
2500
2000
1500
1000
cm-1

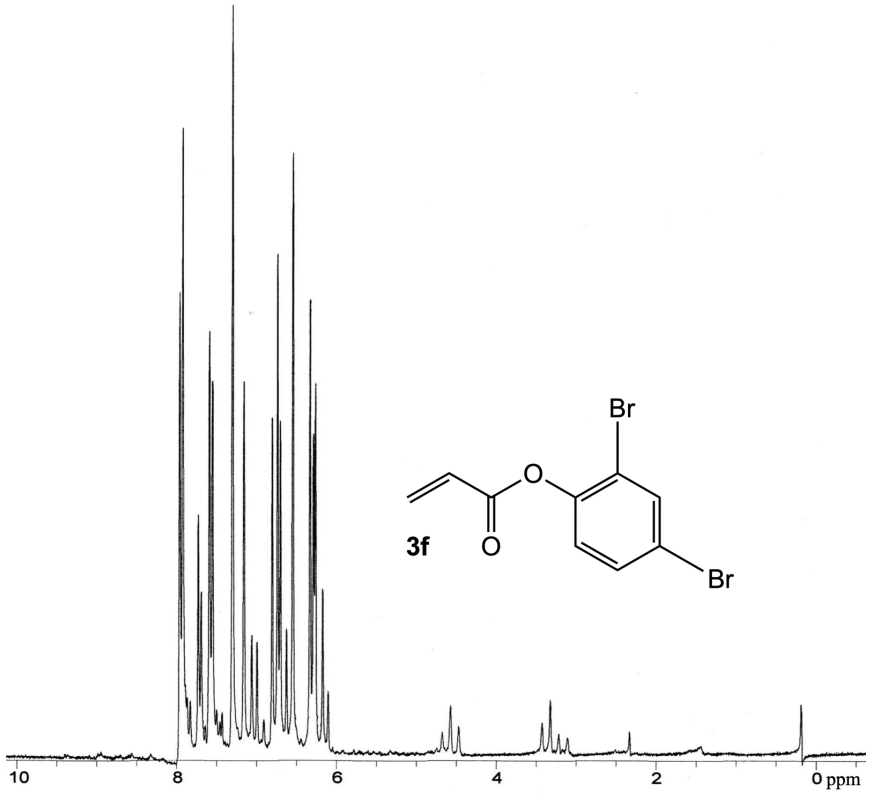
Br
O
3f
O
Br
10
8
6
4
2
0 ppm

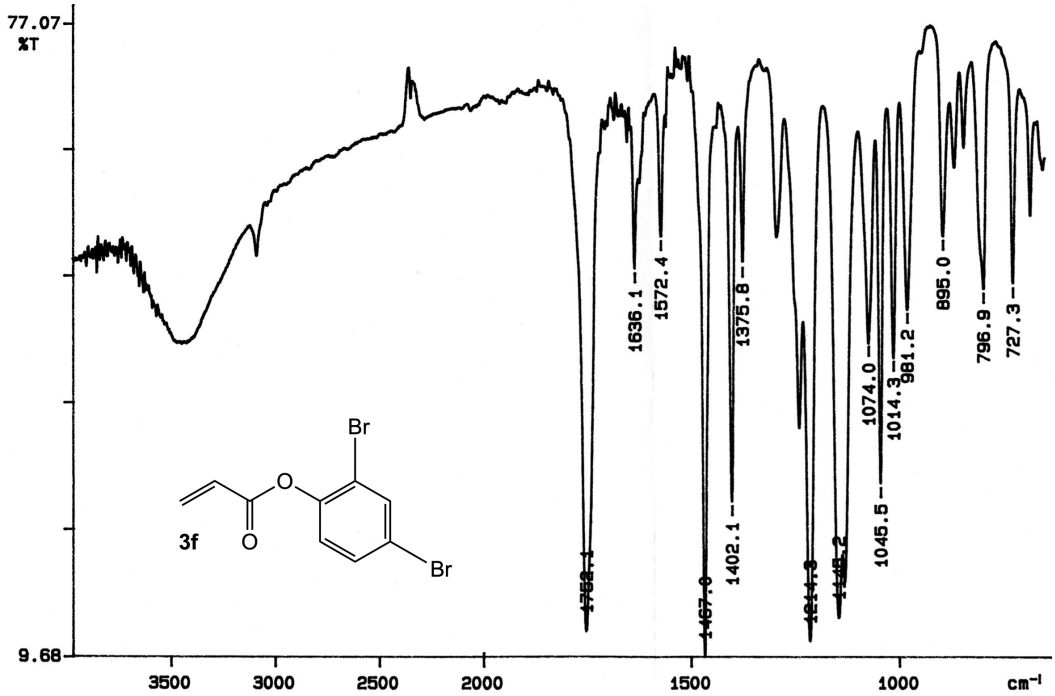
77.07
%T
9.68
1636.1
1572.4
1375.8
1402.1
1074.0
1045.5
1014.3
981.2
895.0
796.9
727.3
Br
O
3f
O
Br
3500
3000
2500
2000
1500
1000
cm-1

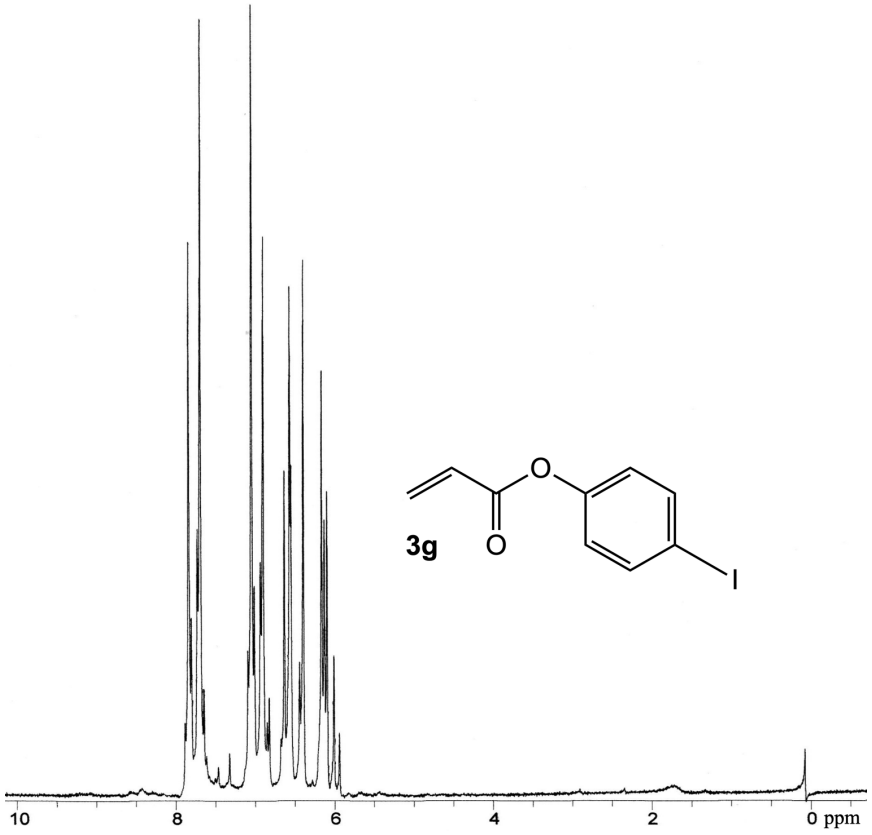
3g
O
O
I
10
8
6
4
2
0 ppm

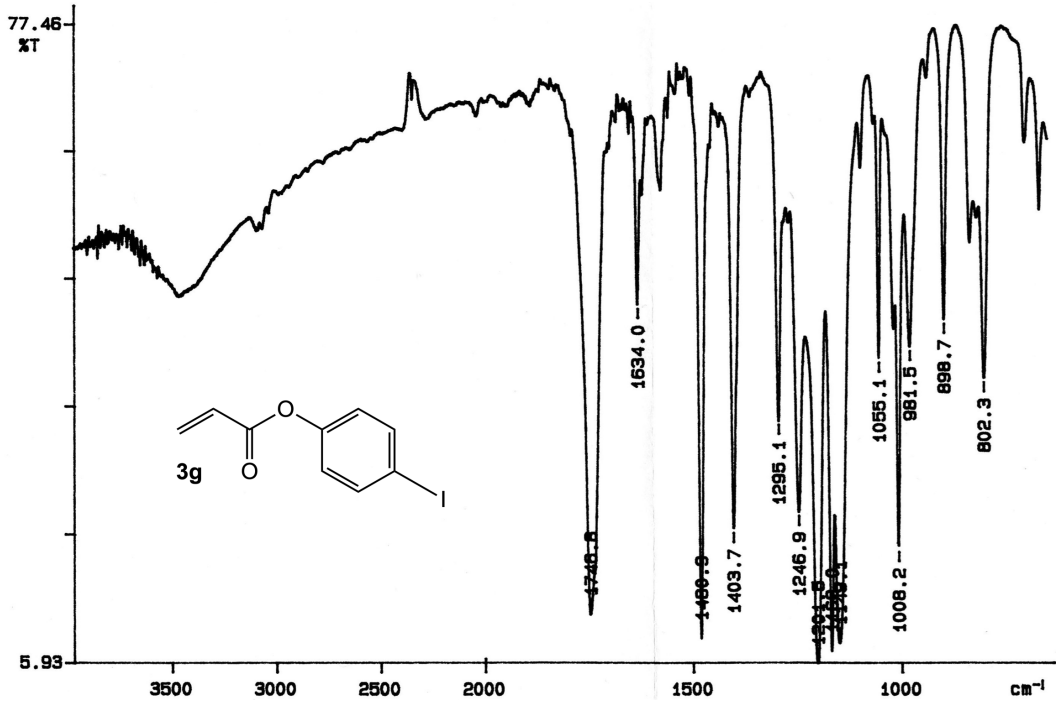
77.46
%T
5.93
3g
O
O
I
1634.0
1403.7
1295.1
1246.9
1055.1
1008.2
981.5
898.7
802.3
3500
3000
2500
2000
1500
1000
cm-1

Data S2. Product Characterization: Related to Table 1.

Phenyl Acrylate (**3a**).

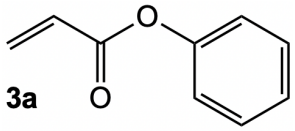

3a

A colorless oil; average isolated yield = 59%; $n_D^{25} = 1.5354$; $\varepsilon_{266\,nm} = 587.18\,M^{-1}cm^{-1}$; $\varepsilon_{313\,nm} = 11.33\,M^{-1}cm^{-1}$; $\varepsilon_{365\,nm} = 4.00\,M^{-1}cm^{-1}$; ^{1}H NMR (60 MHz, NEAT) δ 6.93-7.61 (m, 5H), 5.83-6.59 (m, 3H); IR (ν, cm^{-1}) 1740.3, 1591.5, 1197.9, 982.8, 920.9, 883.3, 691.3; MS (*m*/*z*) 55, 65, 66, 93, 94.

3-Chlorophenyl Acrylate (**3b**).

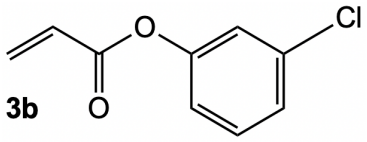

3b

A pale yellow oil; average isolated yield = 33%; $n_D^{25} = 1.5359$; $\varepsilon_{266\,nm} = 761.75\,M^{-1}cm^{-1}$; $\varepsilon_{313\,nm} = 18.74\,M^{-1}cm^{-1}$; $\varepsilon_{365\,nm} = 12.06\,M^{-1}cm^{-1}$; ^{1}H NMR (60 MHz, NEAT) δ 6.71-7.45 (m, 4H), 5.83-6.68 (m, 3H); IR (ν, cm^{-1}) 1747.3, 1589.9, 1209.4, 982.4, 877.1, 778.1, 678.0; MS (*m*/*z*) 55, 58, 67, 72, 94, 105, 112, 127, 156, 180.

4-Chlorophenyl Acrylate (**3c**).

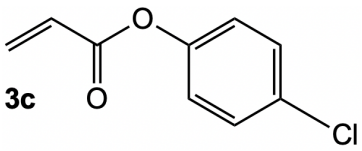

3c

A pale yellow oil; average isolated yield = 36%; $n_D^{25} = 1.5550$; $\varepsilon_{266\,nm} = 454.64\,M^{-1}cm^{-1}$; $\varepsilon_{313\,nm} = 0.42\,M^{-1}cm^{-1}$; $\varepsilon_{365\,nm} = 0.00\,M^{-1}cm^{-1}$; ^{1}H NMR (60 MHz, NEAT) δ 6.92-7.00 (m, 4H), 5.88- 6.91 (m, 3H); IR (ν, cm^{-1}) 1745.0, 1635.4, 1203.0, 982.1, 899.2, 807.2; MS (*m*/*z*) 55, 57, 73, 104, 116, 132, 143, 172.

2,4-Dichlorophenyl Acrylate (**3d**).

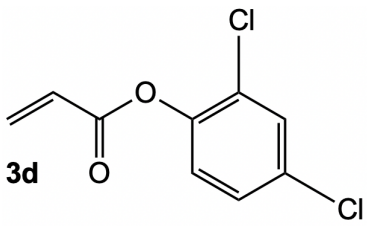

3d

A yellow-orange oil; average isolated yield = 30.%; $n_D^{25} = 1.5900$; $\varepsilon_{266\,nm} = 901.33\,M^{-1}cm^{-1}$; $\varepsilon_{313\,nm} = 0.00\,M^{-1}cm^{-1}$; $\varepsilon_{365\,nm} = 0.00\,M^{-1}cm^{-1}$; ^{1}H NMR (60 MHz, NEAT) δ 6.71-7.53 (m, 3H), 5.97-6.61 (m, 3H);

IR (ν, cm^{-1}) 1751.1, 1583.9, 1218.2, 982.0, 875, 866.0 cm^{-1}, 810.9 cm^{-1}; MS (*m*/*z*) 55, 74, 89, 94, 111, 134, 162, 196, 216, 217, 218, 220.

4-Bromophenyl Acrylate (**3e**).

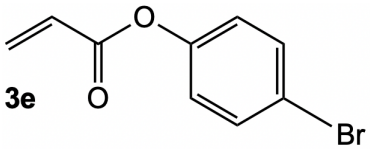

A yellow-orange oil; average isolated yield = 21%; $n_D^{25} = 1.5580$; $\varepsilon_{266\,nm} = 465.11\ M^{-1}cm^{-1}$; $\varepsilon_{313\,nm} = 5.37\ M^{-1}cm^{-1}$; $\varepsilon_{365\,nm} = 0.34\ M^{-1}cm^{-1}$; ^{1}H NMR (60 MHz, NEAT) δ 6.61-7.73 (m, 4H), 5.84-6.58 (m, 3H); IR (ν, cm^{-1}) 1747.9, 1635.4, 1200.5, 981.8, 898.5, 804.5; MS (*m*/*z*) 50, 55, 73, 98, 109, 133, 162, 216.

2,4-Dibromophenyl Acrylate (**3f**).

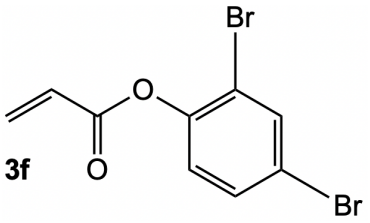

A yellow-orange oil; average isolated yield = 39%; $n_D^{25} = 1.5998$; $\varepsilon_{266\,nm} = 764.62\ M^{-1}cm^{-1}$; $\varepsilon_{313\,nm} = 0.00\ M^{-1}cm^{-1}$; $\varepsilon_{365\,nm} = 0.00\ M^{-1}cm^{-1}$; ^{1}H NMR (60 MHz, NEAT) δ 7.25-7.81 (m, 3H), 5.91-7.23 (m, 3H); IR (ν, cm^{-1}) 1752.1, 1636.1, 1214.3, 981.2, 895.0, 883, 796.9; MS (*m*/*z*) 50, 55, 59, 75, 93, 117, 143, 172, 174, 226, 228, 281.

4-Iodophenyl Acrylate (**3g**).

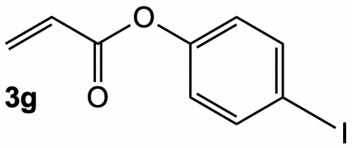

A pale yellow oil; average isolated yield < 10%; $n_D^{25} = 1.5229$; $\varepsilon_{266\,nm} = 3434.39\ M^{-1}cm^{-1}$; $\varepsilon_{313\,nm} = 0.00\ M^{-1}cm^{-1}$; $\varepsilon_{365\,nm} = 0.00\ M^{-1}cm^{-1}$; ^{1}H NMR (60 MHz, NEAT) δ 6.65-8.00 (m, 4H), 5.81-6.64 (m, 3H); IR (ν, cm^{-1}) 1746.6, 1634.0, 1201.5, 981.5, 898.7, 802.3; MS (*m*/*z*) 55, 58, 85, 98, 112, 127, 162, 207.

Data S3. Product Characterization: Homopolymers of phenyl acrylate derivatives, Related to Table 3 and Figures 2-4.

Upon polymerization, the homopolymers of the phenyl acrylate derivatives were analyzed via ATR-FT-IR. Each homopolymer was devoid of vinyl functionality evidenced by the absence of distinguishing vinylic peaks [IR (ν, cm^{-1}) 1633, 984, 920]. Furthermore, the ATR-FT-IR was largely unchanged for the homopolymers over the course of three years when stored in a humidity controlled environment. In other

words, no degradation or delamination of the homopolymer coatings were observed after aging for three years.

ATR-FTIR of poly(phenyl acrylate) (ν, cm^{-1}) 3009, 2970, 1730, 1436, 1366, 1229, 1217, 1206, 903.

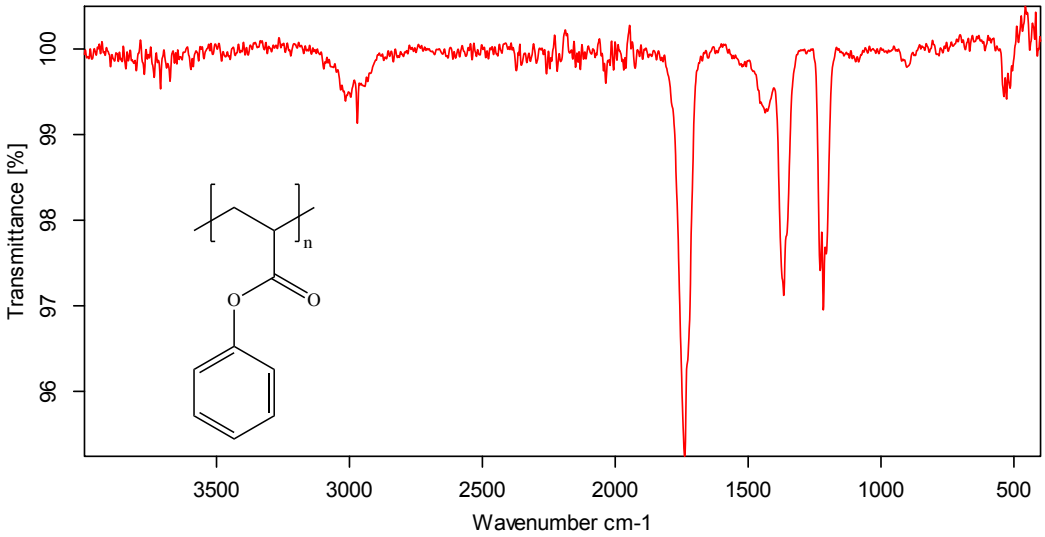

ATR-FTIR of poly(3-chlorophenyl acrylate) (ν, cm^{-1}) 3009, 2970, 1738, 1435, 1366, 1229, 1217, 1206, 893.

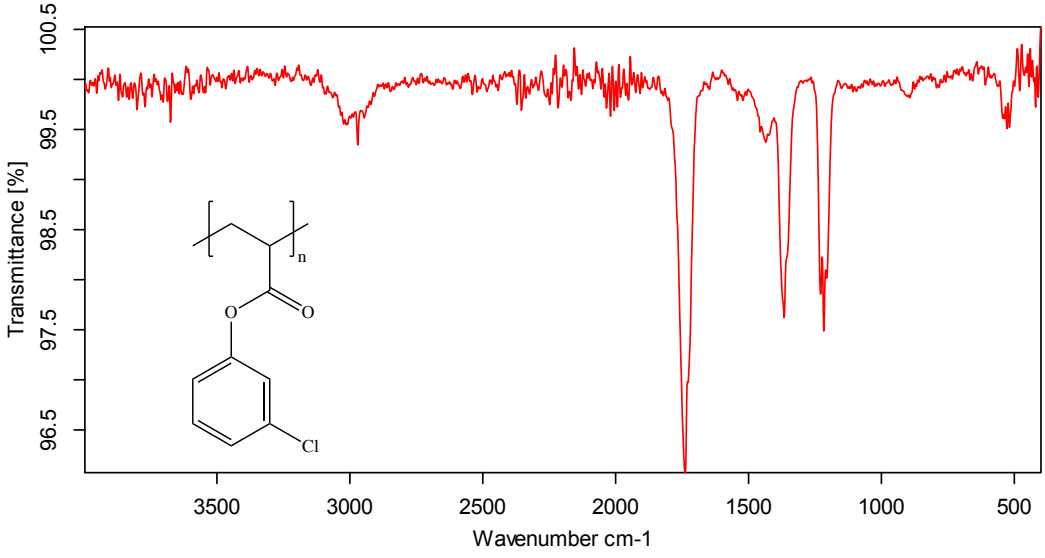

ATR-FTIR of poly(4-chlorophenyl acrylate) (ν, cm^{-1}) 3012, 2970, 1740, 1437, 1366, 1229, 1217, 1206, 905.

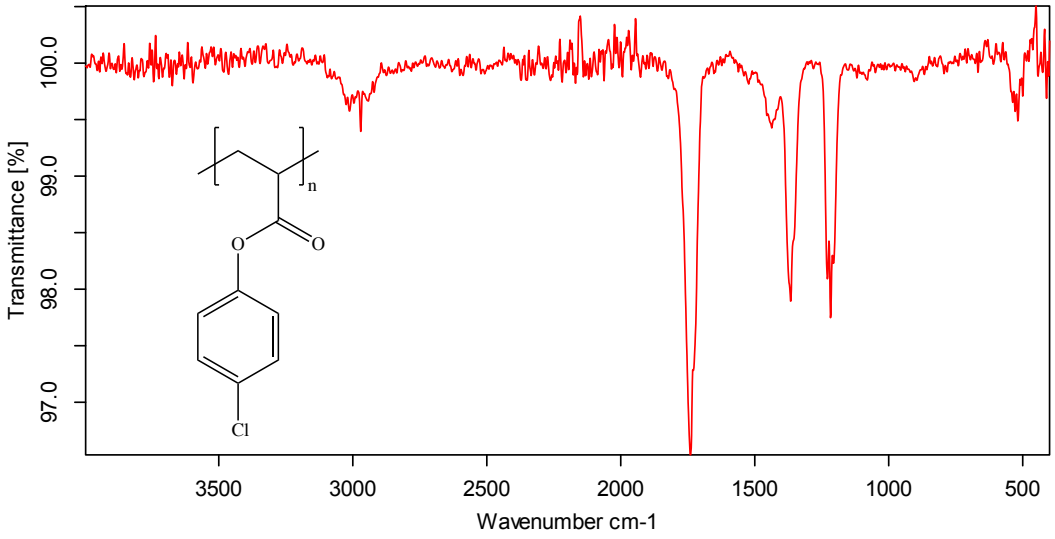

ATR-FTIR of poly(2,4-dichlorophenyl acrylate) (ν, cm^{-1}) 3016, 2970, 1738, 1437, 1366, 1228, 1217, 1206, 903.

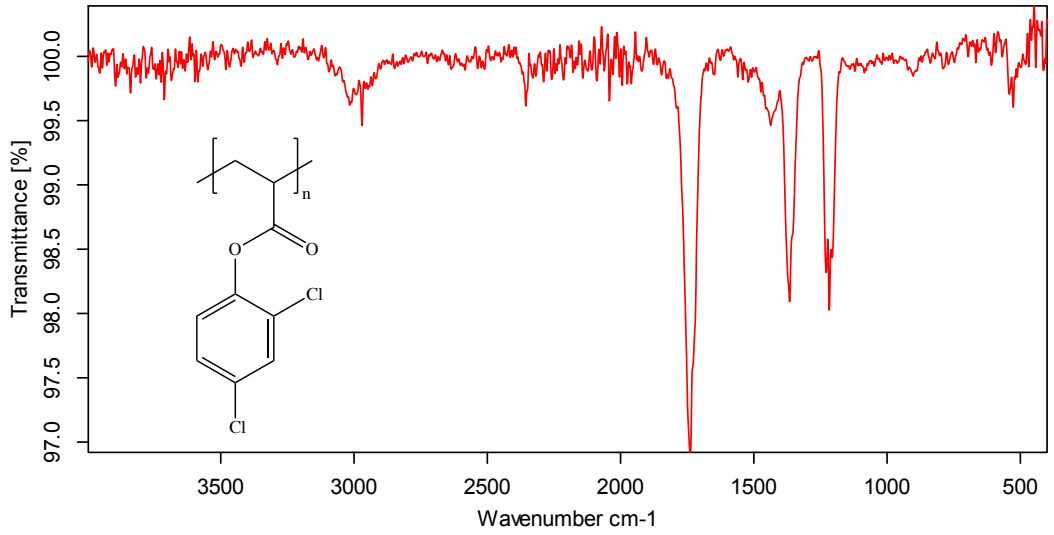

ATR-FTIR of poly(4-bromophenyl acrylate) (ν, cm^{-1}) 3014, 2970, 1738, 1437, 1229, 1217, 1206, 909, 895.

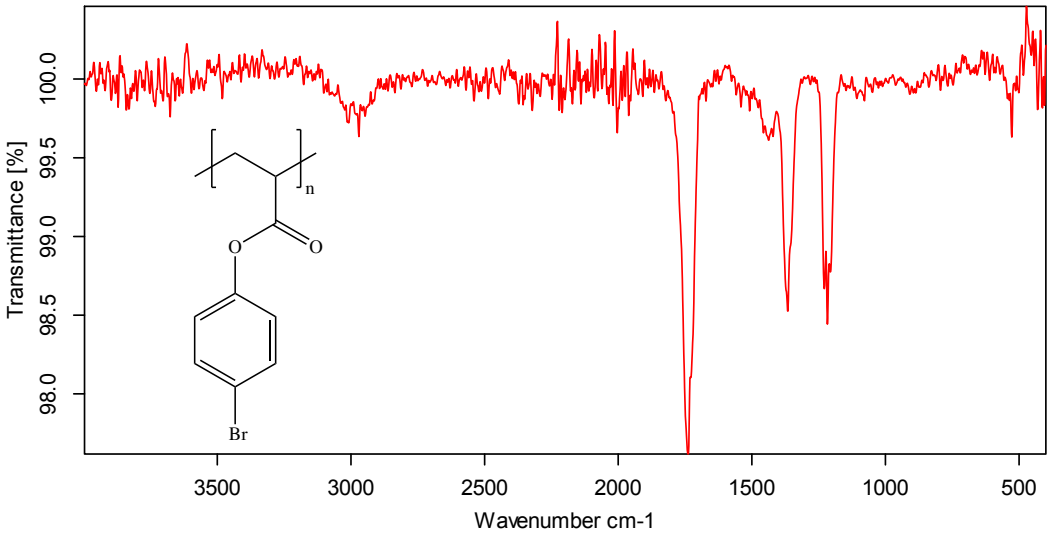

ATR-FTIR of poly(2,4-dibromophenyl acrylate) (ν, cm^{-1}) 3011, 2970, 1740, 1436, 1366, 1228, 1217, 1206, 905, 898.

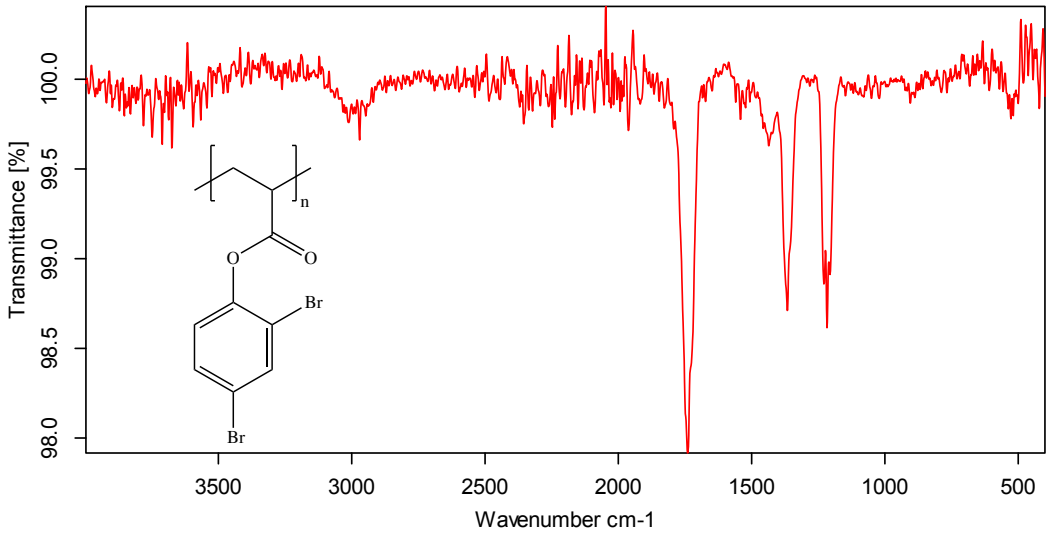

ATR-FTIR of poly(4-iodophenyl acrylate) (ν, cm^{-1}) 3009, 2956, 1738, 1437, 1366, 1227, 1217, 1207, 907.

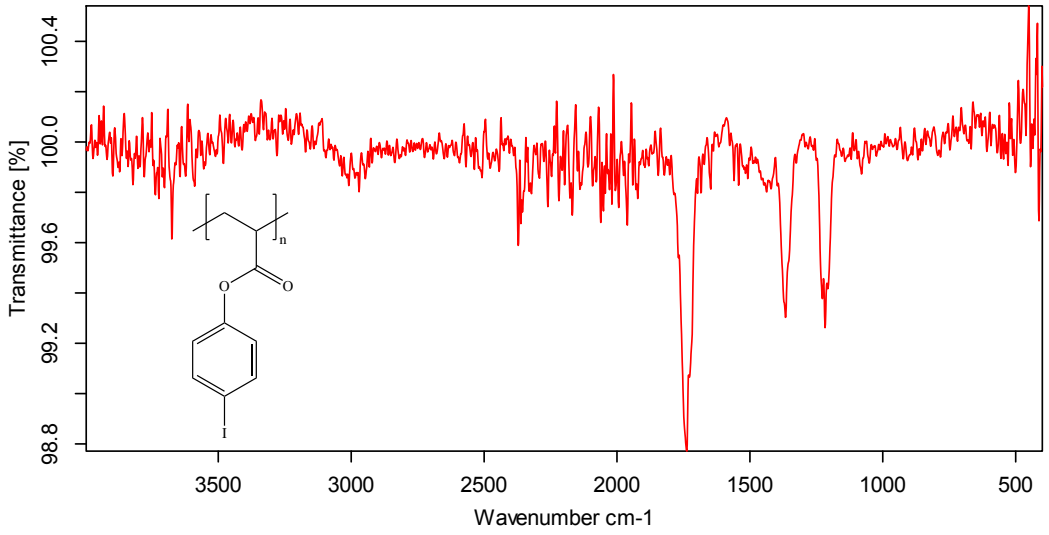

Data S4. Figures associated with Transparent Methods.

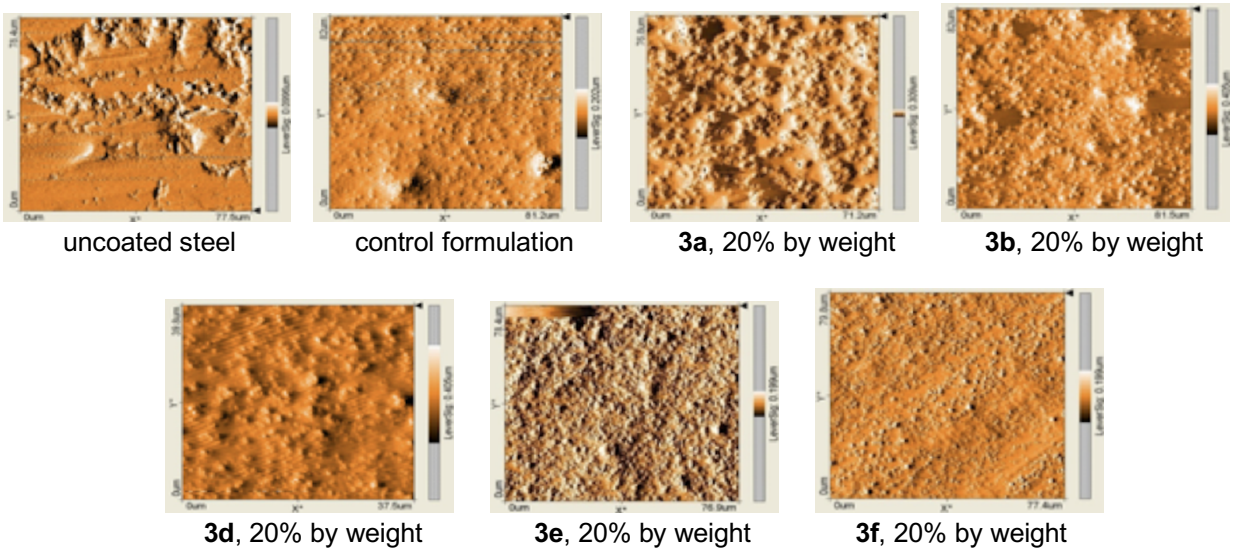

Figure S1. AFM surface profile scans, contact scanning mode, Related to Table 2.

Sample	*E. coli*	*S. aureus*	*P. aeruginosa*	*S. typhimurium*	*S. pneumoniae*
Control coating (uncoated)		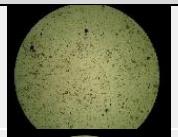			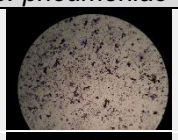
Control coating	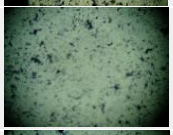		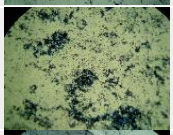	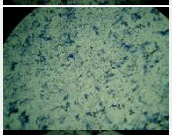	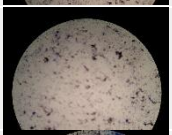
3a control (uncoated)	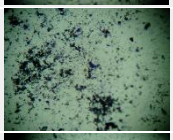	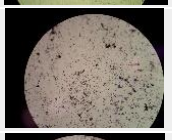	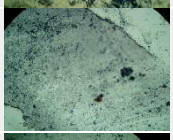	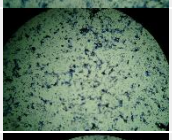	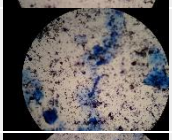
3a	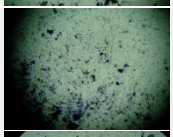	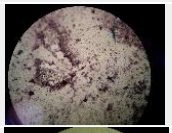	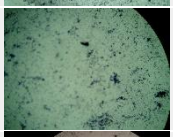	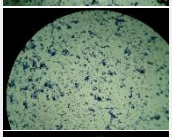	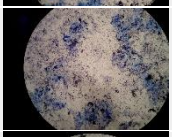
3b control (uncoated)	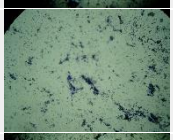	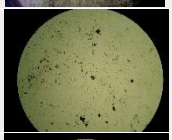	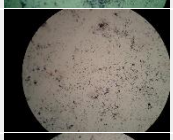	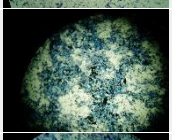	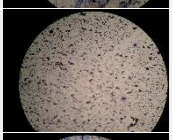
3b	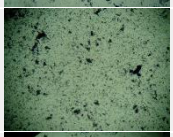	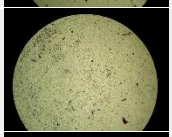	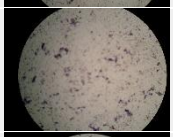	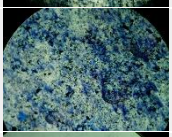	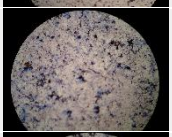
3d control (uncoated)	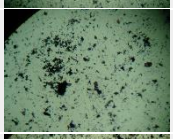	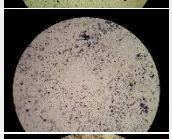	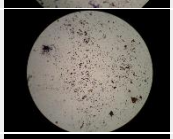	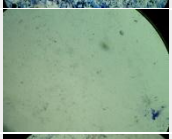	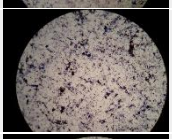
3d	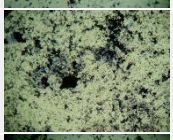	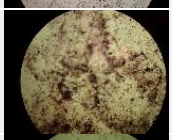	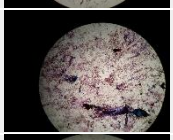		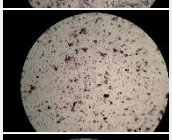
3e control (uncoated)					
3e					
3f control (uncoated)					
3f					

Figure S2. Stained plastic slides of representative monomers (i.e., 3a**,** 3b**,** 3d**,** 3e**, and** 3f**) at 20 weight percent coating incorporation (100x magnification) after biofilm reactor incubation, Related to Figure 1.**

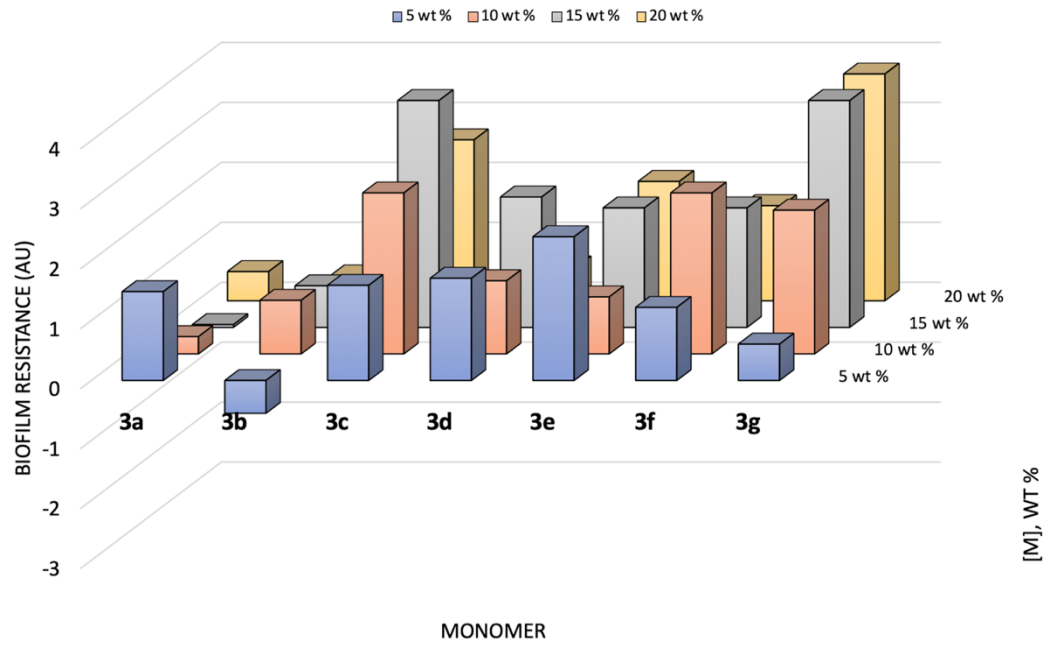

Figure S3. Evaluation of *E. coli* biofilm resistance, Related to Figure 1.

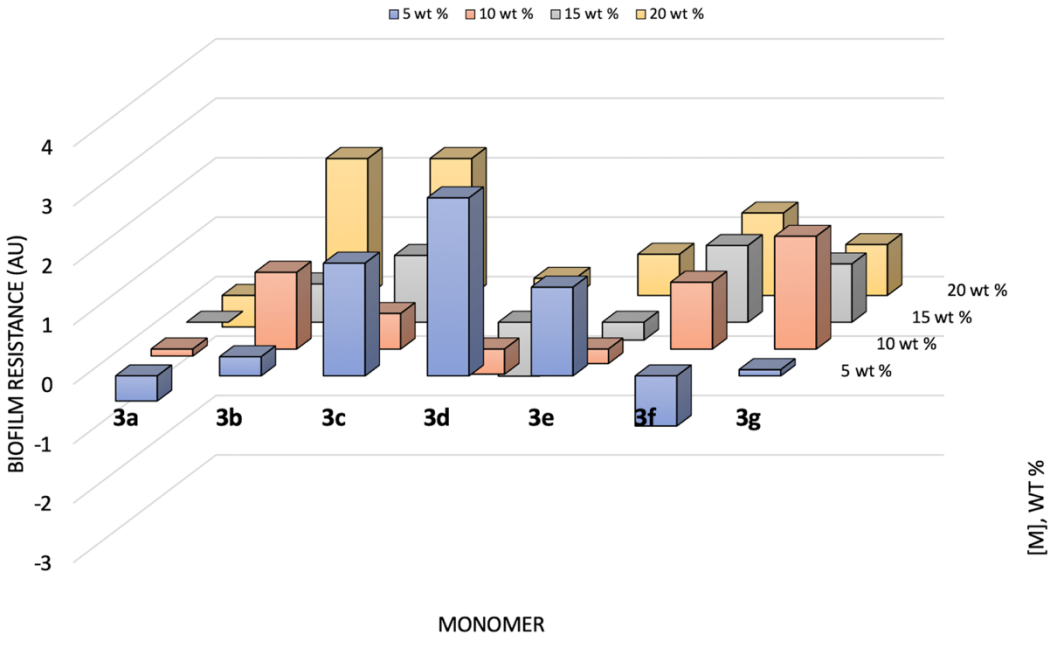

Figure S4. Evaluation of *P. aeruginosa* biofilm resistance, Related to Figure 1.

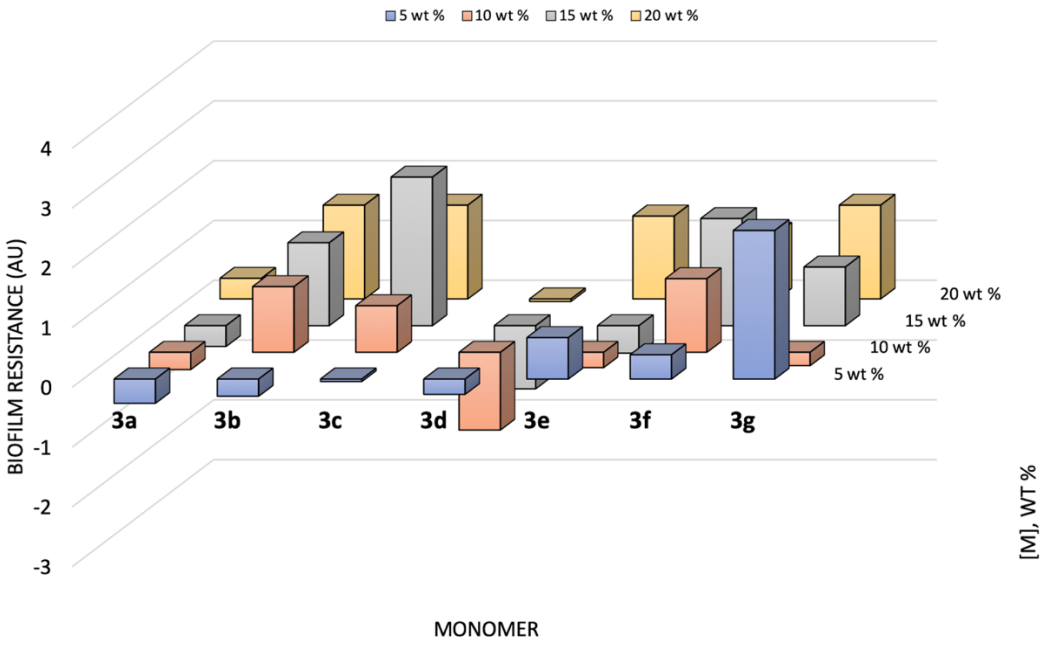

Figure S5. Evaluation of *S. aureus* biofilm resistance, Related to Figure 1.

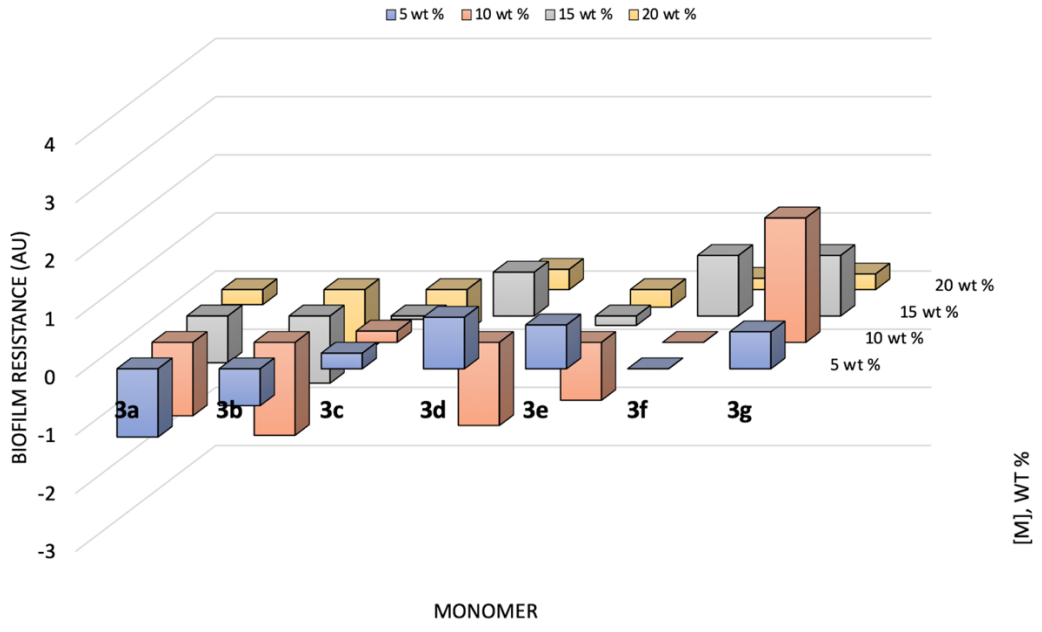

Figure S6. Evaluation of *S. pneumoniae* biofilm resistance, Related to Figure 1.

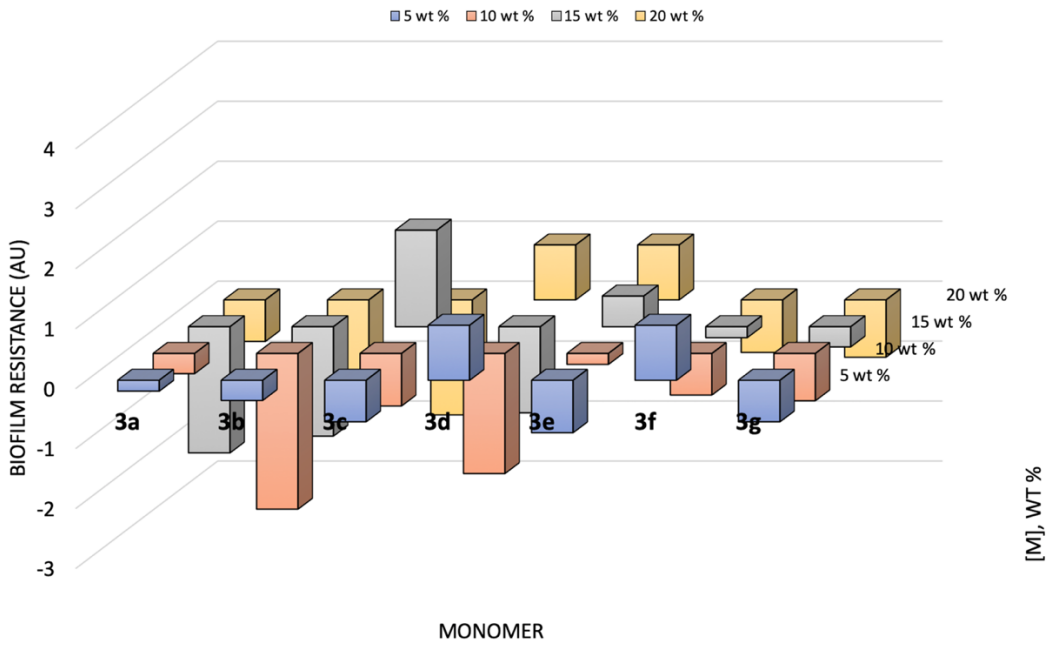

Figure S7. Evaluation of *S. typhimurium* biofilm resistance, Related to Figure 1.

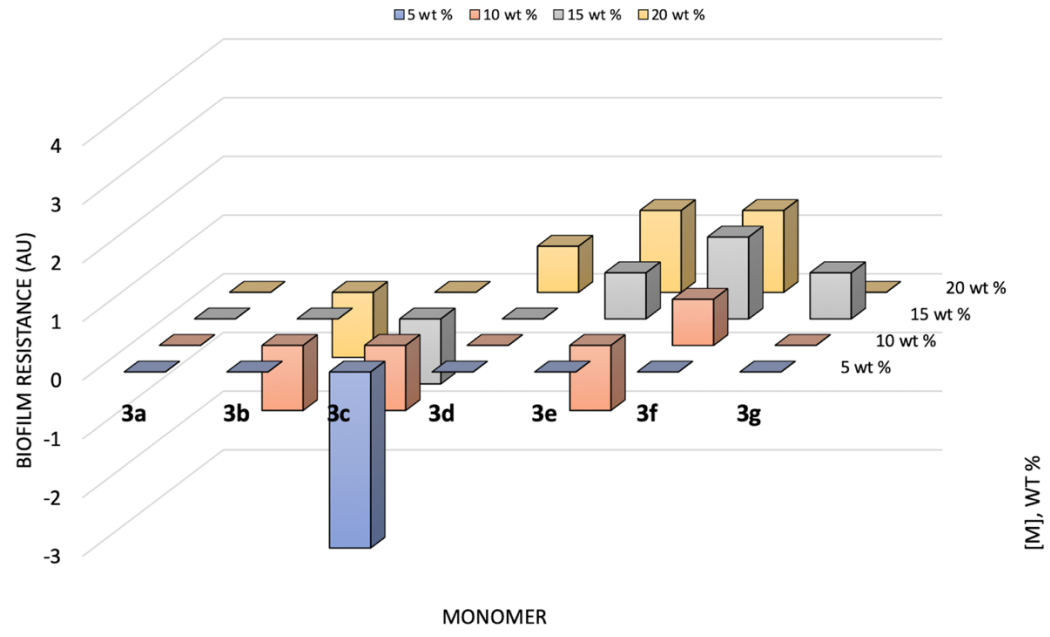

Figure S8. Qualitative evaluation of multiple species biofilm resistance in raw clarified sewage, Related to Figure 1.

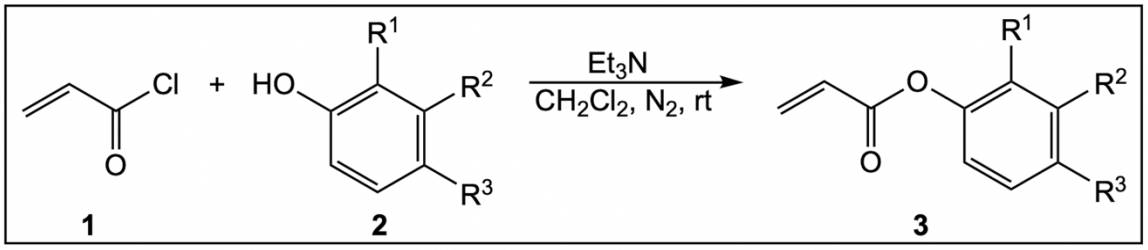

Figure S9. Synthetic reaction scheme, Related to Table 1.

TRANSPARENT METHODS

A. General Information

Materials and Instrumentation.

Most chemicals used in the monomer syntheses and testing, including the phenolic precursors, triethylamine (Et_3N), acryloyl chloride, and acetonitrile, were purchased from Sigma-Aldrich. The dichloromethane also used in the syntheses was purchased from Pharmacia. The material used for the coating formulations was obtained from Allied Photochemical and is a proprietary formulation. Cytec Specialty Chemicals provided the 1,6-hexanediol diacrylate (HDODA) used in the photo-DSC. Albemarle Corporation donated the photoinitiator, 2,2-dimethoxy-2-phenylacetophenone (DMPA). The uncoated, polished stainless-steel plates were purchased from Q Panel Products. Methyl ethyl ketone (MEK) for the double rub test was purchased from The Paint Center. Cytology fixative spray was obtained from Andwin Scientific. Nitrogen gas was provided by Airgas.

The bacteria were stained using Hema-diff solution 3-thiazine dye from Anapath. Bacteria were obtained from Carolina Biological Supply. The Luria-Bertani, Miller (LB Miller) nutrient agar was provided by Fisher Scientific. The Trypticase Soy Agar and Bacto Blood Agar Base, Dehydrated were obtained from Difco. BBL SIM Medium was obtained from BBL Microbiology Systems.

Characterization of monomers and polymers was conducted using multiple machines. The NMR Spectrometer Eft-60 was provided by Anasazi Instruments Inc. The Infrared Spectrophotometer was obtained from Perkin Elmer (1600 Series). The rotary evaporator (Rotovap), collegiate model, was provided by Heidolph LABORTA. Sargent-Welch Scientific Company provided the Welch DuoSeal Vacuum Pump, Model 1400. Mel-Temp Electrothermal melting point apparatus (Model 1201D) was provided by Barnstead/Thermolyne. Refractometer was obtained from Thermo Electron Corporation (Model 334610). Photo-Differential Scanning Calorimeter (DSC 822^e) was obtained from Mettler Toledo and the ultraviolet spot light source was the Lightningcure 200 by Hamamatsu. The Ultraviolet-Visible Spectrometer (HP 8453) was obtained from Hewlett-Packard. Light Microscope (Model M404DP) was provided by Swift Instruments International. AMSCO provided the autoclave model AMSCO 3021 Gravity. Incubation was performed in a GI200A-1 model incubator from Thermo Electron Corporation.

UV-Vis Spectroscopy.

10.0 mL acetonitrile was measured out in a graduated cylinder then added to scintillation vials containing 0.05 g of the monomer. UV-Vis spectra were taken of each monomer then diluted with acetonitrile as

necessary [until absorbance was measured between 0.75-1.0]. Measurements were taken of absorbance at specific wavelengths of the monomers using UV Vis and used to determine the extinction coefficient at wavelengths of 266, 313, and 365 nm.

Coating Production.

Application of Formulation to Unpolished Stainless-Steel Plates. The plates and draw down bar were washed with acetone. The drawdown bar was set in the position demarking four mils (100 μm), and the formulation was applied to the plate along the top edge of the drawdown bar. The drawdown bar was then drawn at uniform speed to evenly apply the coating. If streaking or orange peel occurred, the drawdown was repeated until the formulation was evenly applied.

Application of Formulation to Plastic Slides. Six one-inch by three-inch (1 in. x 3 in.) plastic (optically clear vinyl) slides were prepared per coating formulation. Six slides were laid horizontally together to form a solid plastic surface with the sides taped down. The drawdown bar was placed on the slides and formulation was applied to the top-most slides. The drawdown bar was observed to be in the four mil position and drawn down at uniform speed to evenly coat half of the surface of each of the six slides. If streaking or orange peel occurred, the drawdown was repeated until the formulation was evenly applied.

Application of Formulation to Glass Slides. One, one-inch by three-inch (1 in. x 3in.) glass slide was prepared per formulation. Four glass slides were laid down vertically to form two columns of two slides each far enough apart to fit a fifth glass slide in the middle (the one to be coated) and to allow the edges of the draw down bar to rest on them. In this manner a uniform coating depth was achieved for the targeted glass slide because the drawdown bar rested not on the experimental surface, but on glass slides of the same size as the target. When the drawdown bar was placed on the supporting glass slides and observed to be in the four mil position, formulation was applied to the target glass slide. The drawdown bar was drawn at a uniform speed to spread the formulation evenly; however, if streaking or orange peel occurred, the drawdown was repeated.

Polymerization of phenyl acrylate monomer derivatives. Multiple passes under a Fusion UV Systems, Inc. LC-6/F300S equipped with a H-bulb cured the formulations (one weight percent DMPA dissolved in monomer) in air at 20 feet per minute and were confirmed via a traditional thumb-twist test. The coatings were cured to metal plates, plastic slides, and glass slides to conduct various physical and biological tests.

Biologic sample preparation for contact angle measurements. Bovine collagen (purchased from Aldrich) coatings were prepared according to established literature protocols (Hansen et al., 2011). For consistency, insoluble and soluble collagen concentrations were measured to be 100 μg/mL. Soluble collagen was dissolved in a phosphate buffer system (1 x PBS, pH = 7.4) purchased from Aldrich.

Both *S. aureus* and *P. aeruginosa* were rehydrated according to established procedures from the supplier and transferred aseptically onto two 10 mL Luria-Bertani (LB), Miller, nutrient agar plates. The inoculated plates were placed in an incubator at 37°C for 72 hours. After incubation, the specimens were placed in a refrigerator and stored at 6°C until use.

Atomic Force Microscopy (AFM): Related to Table 2.

Atomic force microscopy (AFM) contact scanning curves of each coating were obtained at two locations that were an approximate 80 μm x 80 μm area (6,400 μm^2) to eliminate the effects of interference on the roughness measurements. Both X and Y roughness calculations were averaged to yield the average three-dimensional surface roughness (R_a) for each location (Equation S1) (Raposo et al., 2007).

$$R_a(M,N) = \frac{1}{NM}\sum_{x=1}^{N}\sum_{y=1}^{M}[z(x,y) - \overline{z}(x,y)] \quad \text{(S1)}$$

Three locations were arbitrarily selected for each plate whereupon the roughness and peak-valley height (R_z) were determined (Equation S2) (Raposo et al., 2007).

$$R_z = \frac{1}{n}\left(\sum_{i=1}^{3} R_{p,i} + \sum_{i=1}^{3} R_{v,i}\right) \quad \text{(S2)}$$

The roughness values and peak-valley height for the three locations were then all averaged for an overall average plate roughness and average peak-valley height. The average peak-valley height was then compared to that of surgical grade steel ($R_z \leq 1$ μm). Scans of both controls and cured copolymers at 20 weight percent monomer incorporation are shown in Figure S1.

Extraction Studies.

Extraction studies were performed for all cured formulations at 20 weight percent active monomer incorporation using gas chromatography (GC) – mass spectrometry (MS). Each cured coating (0.5 g) was scraped from the steel plates, powdered, placed into 10 mL of methanol in a capped vial, and allowed to soak for one week at which point one milliliter of the supernatant was placed into a GC sample vial. The GC-MS was then run for each of the samples whereupon the percent extractables were calculated. The lower limit of detection is 100 µg/mL. The GC used a 30 m (0.1 mm inside diameter) nonpolar column with a 250°C injection temperature, 150°C oven temperature, and 280°C interface temperature.

Photo-Differential Scanning Calorimetry (Photo-DSC).

The monomers (i.e., phenyl acrylate derivatives, **3a-g**) were formulated at ten weight percent with one weight percent DMPA in HDODA, and then two microliters (2 μL) of each formulation was measured into crimped, aluminum sample pans. The light intensities were measured using black body absorbers. The calorimetric measurements were performed using a Mettler-Toledo DSC 822^e modified with a Hamamatsu Lightning Cure 200 UV-spot, equipped with a full-arc high-pressure mercury lamp. The sample cell was kept at a constant 20°C by a Julabo FT 100 intercooler. The sample was purged with nitrogen for two minutes prior to beginning the run and continued through the completion of the run. The polymerization rates of each monomer were compared to that of *NEAT* HDODA and to a HDODA sample photoinitiated by a standard *Norrish Type I* photoinitiator (e.g., DMPA). No increased polymerization rate for all samples indicate persistence of the aryl halide in the final polymerized sample.

Single Species Biofilm Resistance Studies: Related to Figure 1.

The ability of microorganisms to form biofilms on the coatings was tested through the cultivation of five different bacteria and subsequent exposure of these microorganisms to the coatings.

Cultivation. All specimens were rehydrated according to established procedures from the supplier. The rehydrated bacteria (*Escherichia coli*, *Staphylococcus aureus*, *Salmonella typhimurium*, and *Pseudomonas aeruginosa*) were transferred aseptically into four test tubes containing 10 mL LB, Miller, nutrient agar slants. The inoculated test tubes were placed in an incubator at 37°C for 72 hours. After incubation, the specimens were placed in a refrigerator and stored at 6°C until use.

Streptococcus pneumoniae was cultivated within an agar composed of 45% Trypticase™ Soy Agar, 30% Blood Base Agar, and 25% BBL SIM agar. Due to the fastidious nature of *S. pneumoniae*, *S. pneumoniae* was the only specimen cultivated anaerobically in six plates composed of 10mL each of the aforementioned

custom agar and in four test tube slants containing 10 mL of the custom agar. The inoculated samples were placed in an incubator at 37°C for 72 hours and afterward stored in a refrigerator at 6°C.

Induction of Biofilm Formation. A biofilm reactor was built to characterize the biofilm resistance of coatings within a bacteria rich environment. A fish tank (30 inches in length, 12.25 inches wide, and 12.5 inches high) was divided into five equally sized sections using custom cut poly(methyl methacrylate) sheets and sealed with waterproof sealant to prevent cross contamination. An evaporative cooler pump was placed in each compartment to circulate approximately three liters of bacterial broth in each compartment. The solution was composed of 3000 mL sterilized water with three grams of LB, Miller, nutrient agar. Each bacterial strain was cultivated in 100 mL of water and 0.3 g of LB, Miller, nutrient agar at 37°C for 24 hours. After 24 hours the inoculated broths were poured into corresponding sections of the biofilm reactor. Plastic slides containing each of the coating formulations were simultaneously placed in the reactor on a holding apparatus built to allow for a flow assay to measure biofilm growth. In other words, biofilm growth was performed in bulk upon every sample simultaneously. Each plastic slide was divided into an uncoated side (internal control) and a coated side (measuring biofilm growth). Over the course of 10 days, 500 mL of broth was replaced with 500 mL sterilized water each day. After this 10 day period, the holding apparatus and all slides were removed as one. The unattached bacteria and any other materials were rinsed from the slides with sterile, deionized water. The slides were sprayed with a cytology fixative [poly(ethylene glycol)-based]. After the fixative was air dried, the slides were rinsed with deionized water, and stained with methylene blue/Azure A. The excess dye was removed with sterile water leaving behind any residual stained bacteria on the slide. Representative stained samples are provided in Figure S2.

Upon cultivating single species biofilms in the custom-built biofilm reactor, qualitative examination of coated plastic slides was performed via optical microscopy (100x magnification) to ascertain success of the biofilm resistant polymers after staining. Quantitative evaluation of the biofilm resistance of the phenyl acrylate monomers relative to the bacterium were determined via colony forming unit (CFU) count. All CFU counts are relative to the control coating with no phenyl acrylate monomer derivatives present (Figures S3-S7 scaled identically).

Figures S3-S7 are quantitatively normalized relative to biofilm growth on the control coating [i.e., UV-curable semi-gloss acrylic clearcoat (Allied Photochemical, KZ-7025-CL)]. Reduced biofilm resistance relative to the control is negative while increased biofilm resistance is positive. Biofilms for Figures S3-S5 and S7 were cultured for 10 days at 38ºC in LB Miller agar broth under starvation conditions. Likewise, the biofilm related to Figure S6 was cultured; however, the broth used was a blood-based soy agar.

Some biofilm resistance was observed for monomers **3c-g**; however, monomers **3a** and **3b** did not exhibit any appreciable *E. coli* biofilm resistance. While the lack of biofilm resistance for **3a** was expected, that of **3b** might indicate that *meta*-chlorination promotes limited biofilm resistance toward *E. coli*. Some biofilm resistance was observed for **3d**. With a direct relationship of monomer concentration to biofilm resistance, **3c**, **3f**, **3e**, and **3g** demonstrated significant biofilm resistance. Also, *para*-halogenation seems to increase biofilm resistance for *E. coli*. The heavier brominated and iodinated monomers were generally better biofilm inhibitors than the chlorinated derivatives.

P. aeruginosa is among the best biofilm forming bacteria and was a logical choice for demonstrating biofilm resistance. The chlorinated monomers (**3b**, **3c**, and **3d**) exhibited more significant biofilm resistance to *P. aeruginosa* than the brominated or iodinated monomers. However, at higher concentrations of the brominated (**3e** and **3f**) or iodinated (**3g**) monomers, biofilm resistance increased. Interestingly, **3d** was more efficacious at lower concentrations indicating that the biostatic effect inherent to a MIC may be a more important effect for this bacterium than ensuring a cidal effect via MBC.

The monochlorinated monomers (**3b** and **3c**), especially at increased concentrations, inhibited biofilm development of *S. aureus*; yet, **3d** did not exhibit appreciable biofilm resistance. At increasing concentrations of the brominated monomers (**3e** and **3f**), biofilm resistance increased noticeably indicating a direct concentration correlation. Both **3e** and **3g** had a biostatic effect similar to that previously described for **3d** with *P. aeruginosa*.

Across the board, less biofilm resistance was observed for the monomers toward *S. pneumoniae* lower monomer concentrations (≤15 weight percent) did not inhibit biofilm formation. Three derivatives (e.g., **3d**, **3f**, and **3g**) exhibited moderate biofilm resistance with **3g** being most effective. Again **3e** showed a biostatic effect. Multihalogenated monomers and softer atoms (e.g., bromine and iodine) seem to be most effective at inhibiting *S. pneumoniae* biofilm formation.

Moderate biofilm inhibition was observed for the 15 weight percent concentration of **3c**. *S. typhimurium* biofilms were most inhibited by the dichlorinated (**3d**) and monobrominated (**3e**) monomers at several concentrations. **3f** had a slight biostatic effect at low concentration. No clear trend was observed for biofilm inhibition of *S. typhimurium*.

Multiple Species Biofilm Resistance Studies.

A multiple species biofilm resistance study for each coating was performed by immersion into sedimented (i.e., clarified) raw sewage in the secondary clarifiers at the Abilene Wastewater Reclamation Plant in Abilene, Texas.

Each cured slide was hot glued to a poly(methyl methacrylate), PMMA, sample sheet obtained from a local home improvement store. The sample sheet was placed into another custom-built apparatus resembling a metal cage, termed the biofilm resistance apparatus (BRApp), in order to protect the samples from mechanical processes that could remove either the coating or the grown biofilm.

Then, the BRApp was taken to the Abilene Wastewater Reclamation Plant and submerged into the secondary clarifier which allows the aerated raw sewage to grow existing microbes, some of which consume a portion of the raw sewage materials. It is important to note that the bulk of the solid sewage was removed via sedimentation in the primary clarifiers prior to aeration. Each secondary clarifier is capable of handling 1.75 million gallons of raw sewage each day. The BRApp was left in the secondary clarifier for two days (3.5 million gallons of total exposure) at about a six foot depth, just above the paddle arm that mixes the contents at a rate of six revolutions per hour and ambient outside temperature.

The BRApp was removed and transported back to the lab in a plastic bag whereupon the PMMA sheet was removed, rinsed with deionized water, and treated with an ethanol spray to kill the microbes attached to the sheet and samples. The microbes were then fixated with a poly(ethylene glycol) cytological spray and allowed to dry. Then the slides were stained with a methylene blue/Azure A solution. Each stained slide was qualitatively evaluated by comparing each coating relative to the uncoated portion of the slide both with the naked eye and through an optical microscope (100x) in three different locations on the coating and scaled accordingly [e.g., scale: 1 (excessive biofilm) – 3 (same as control) – 5 (minimal biofilm)]. Data are aggregated in Figure S8 which was qualitatively normalized relative to biofilm growth on the control coating [i.e., UV-curable semi-gloss acrylic clearcoat (Allied Photochemical, KZ-7025-CL)]. Reduced biofilm resistance relative to the control is negative while increased biofilm resistance is positive.

Similar to the laboratory-based, single bacterium studies and after exposure to 3.5 million gallons of raw clarified sewage, the coatings incorporating the brominated monomers (**3e** and **3f**) were most efficacious as biofilm resistant materials. Likewise, the dihalogenated (**3d** and **3f**) compounds seemed to also be more effective biofilm resistant monomers than the monohalogenated monomers of which **3g** exhibited some biofilm resistance unlike the monochlorinated monomers (**3b** and **3c**).

B. Representative Procedures

General Procedure for Synthesis of 3: Related to Table 1.

The phenolic derivative was dissolved in a slight molar excess of triethylamine (TEA) and then added to a 250 mL round bottom flask with 40 mL dichloromethane. Acryloyl chloride (equimolar amount compared to TEA) was added dropwise to the mixture with stirring (Table 1). After the flask was provided with a nitrogen atmosphere the mixture was stirred for 24 hours and thereafter suction filtered to remove the TEA hydrochloride salt. The resulting solution was washed in a separatory funnel 15 times with 15 mL deionized water then anhydrous magnesium sulfate ($MgSO_4$) was added until clumping stopped. The mixture was suction filtered to remove the anhydrous $MgSO_4$ and thereafter placed on the Rotovap for solvent volume reduction. The remaining liquid acrylate was dried via vacuum for 24 hours. The reaction scheme is provided in Figure S9.

NOTE: **3g** was a difficult synthesis and required multiple scaled-up reactions to acquire an adequate amount of the compound for testing; therefore, the corresponding reported average isolated yield is low and not comparative to the other syntheses.

C. Surface Energy Calculations: Related to Tables 3 and 4 and Figures 2-4

While surface energy analyses have many forms, we have chosen one that is arguably the simplest analyses and has historically been used to describe biological systems (Owens et al., 1969; Schrader, 2002; van Oss et al., 1987; van Oss et al., 1988). According to Equation S3, the change in Gibbs energy of an interface ($\Delta G_{interface}$) is directly related to the surface energy of an interacting material (γ_m) (van Oss et al., 1988).

$$\Delta G_{interface} = \left(1 + cos\ \theta_{interface}\right)\gamma_m \quad \text{(S3)}$$

Equation S4 defines γ_m (generically represented as γ^{tot}) to be the sum of the material's individual nonpolar (γ^{LW}) and polar (γ^{AB}) components where γ^{AB} is defined to be the geometric mean of the separate acid (γ^{+}) and base (γ^{-}) components (Equation S5) (van Oss et al., 1988).

$$\gamma^{tot} = \gamma^{LW} + \gamma^{AB} \quad \text{(S4)}$$

$$\gamma^{AB} = 2\sqrt{\gamma^{+}\gamma^{-}} \quad \text{(S5)}$$

Using two fully characterized liquid materials, the Owens-Wendt equation (S6) allows the determination of multiple surface energy components of a substrate (e.g., γ_s^{LW}, γ_s^{AB}, and γ_s) via contact angle (θ_{sl}) (Owens et al., 1969; Schrader, 2002).

$$(1 + cos\ \theta_{sl})\gamma_l^{tot} = 2\left(\sqrt{\gamma_s^{LW}\gamma_l^{LW}} + \sqrt{\gamma_s^{AB}\gamma_l^{AB}}\right) \quad \text{(S6)}$$

The van Oss-Chaudhury-Good (OCG) equation (S7) expands Equation S6 to similarly delineate the substrate's separate acid (γ_s^{+}) and base (γ_s^{-}) components using three fully characterized liquids. Both γ_s^{AB} and γ_s can be determined sequentially via Equations S4 and S5 (van Oss et al., 1987; van Oss et al., 1988).

$$(1 + cos\ \theta_{sl})\gamma_l^{tot} = 2\left(\sqrt{\gamma_s^{LW}\gamma_l^{LW}} + \sqrt{\gamma_s^{+}\gamma_l^{-}} + \sqrt{\gamma_s^{-}\gamma_l^{+}}\right) \quad \text{(S7)}$$

Using a linear algebraic method to simultaneously solve for components, we used Equation 1 to determine the surface energy profile (e.g., γ_s^{LW}, γ_s^{AB}, γ_s^{+}, γ_s^{-}, and γ_s) of each polymerized halogenated monomer.

Contact angle measurements.

The sessile drop method was utilized where a 2 µL droplet was placed on a surface and allowed to equilibrate for one minute. Following equilibration, the drop was photographed using a mounted second generation iPad Mini equipped with a macrolens. Contact angle measurements were obtained via a protractor app (Photo Protractor). To maintain quality control, the contact angle photographs were printed and secondarily validated manually via a physical protractor. Statistical averages for each contact angle measurement (N ≥ 8) were obtained after omitting the statistical outliers. We used bromonaphthalene, dimethylsulfoxide, formamide, and/or water to obtain contact angles used to determine the surface energy profiles.

Linear algebraic determination of surface energy profiles.

A linear algebraic approach could be used to solve Equation S7 as given below using the complete characterization of the solvents used. After obtaining the contact angle measurements, Equation S8 was rearranged to yield Equation S8:

$$\frac{1}{2}[(1+cos\ \theta_{sl})\gamma_l^{tot}] = \sqrt{\gamma_l^{LW}\gamma_s^{LW}} + \sqrt{\gamma_l^{-}\gamma_s^{+}} + \sqrt{\gamma_l^{+}\gamma_s^{-}} \quad \text{(S8)}$$

We then represent the experimentally determined or known values as *a*, *b*, *c*, and *d* and the unknown substrate values as *x*, *y*, and *z* (Equation S9).

$$d = (a \cdot x) + (b \cdot y) + (c \cdot z) \quad \text{(S9)}$$

where the corresponding contact angle measurement for a peculiar liquid is related to its characterized surface energy profile. Furthermore, *d* is defined to be $\frac{1}{2}[(1+cos\ \theta_{sl})\gamma_l^{tot}]$, *a* is $\sqrt{\gamma_l^{LW}}$, *x* is $\sqrt{\gamma_s^{LW}}$, *b* is $\sqrt{\gamma_l^{-}}$, *y* is $\sqrt{\gamma_s^{+}}$, *c* is $\sqrt{\gamma_l^{+}}$, and *z* is $\sqrt{\gamma_s^{-}}$. We can now combine all values in matrix form.

$$\begin{matrix}\text{bromonaphthalene}\\ \text{formamide OR dimethylsulfoxide}\\ \text{water}\end{matrix} \begin{vmatrix} d \\ h \\ l \end{vmatrix} = \begin{vmatrix} a & b & c \\ e & f & g \\ i & j & k \end{vmatrix} \cdot \begin{vmatrix} x \\ y \\ z \end{vmatrix}$$

The 3x1 vector *dhl* (i.e., *d*), 3x3 matrix (i.e., *A*), and 3x1 vector *xyz* (i.e., *x*) can then be represented more simply as Equation S10.

$$d = A \cdot x \quad \text{(S10)}$$

After performing an allowed matrix inversion, we can solve for *x* which gives us values for the substrate's heretofore unknown surface energy components: γ_s^{LW}, γ_s^{+}, and γ_s^{-} (Equation S11).

$$x = A^{-1} \cdot d \quad \text{(S11)}$$

Using the calculated component values, the substrate's acid-base component (γ_s^{AB}) and overall surface energy (γ_s) can be determined using Equations S5 and S4, respectively.

SUPPLEMENTAL RESOURCES

Hansen, R. R.; Tipnis, A. A.; White-Adams, T. C.; Di Paola, J. A.; Neeves, K. B. (2011). Characterization of Collagen Thin Films for von Willebrand Factor Binding and Platelet Adhesion. Langmuir. 27, 22, 13648-13658.

Owens, D.; Wendt, R. Estimation of the Surface Free Energy of Polymers. (1969). J. Appl. Polym. Sci. 13, 1741-1747.

Raposo, M.; Ferreira, Q.; Ribeiro, P. A. (2007). A Guide for Atomic Force Microscopy Analysis of Soft Condensed Matter. In Modern Research and Educational Topics in Microscopy, A. Méndez-Vilas and J. Díaz, eds. (FORMATEX). 758-769.

Schrader, M. E. (2002). Young-Dupré Revisited. Langmuir. 11, 9, 3585–3589.

van Oss, C. J.; Chaudhury, M. K.; Good, R. J. (1987). Monopolar Surfaces. Adv. Colloid Interface Sci. 28, 35-64.

van Oss, C. J.; Good, R. J.; Chaudhury, M. K. (1988). Additive and Nonadditive Surface Tension Components and the Interpretation of Contact Angles. Langmuir. 4, 4, 884-891.